Cell Reports

Article

Human telomerase is directly regulated by non-telomeric TRF2-G-quadruplex interaction

Graphical abstract

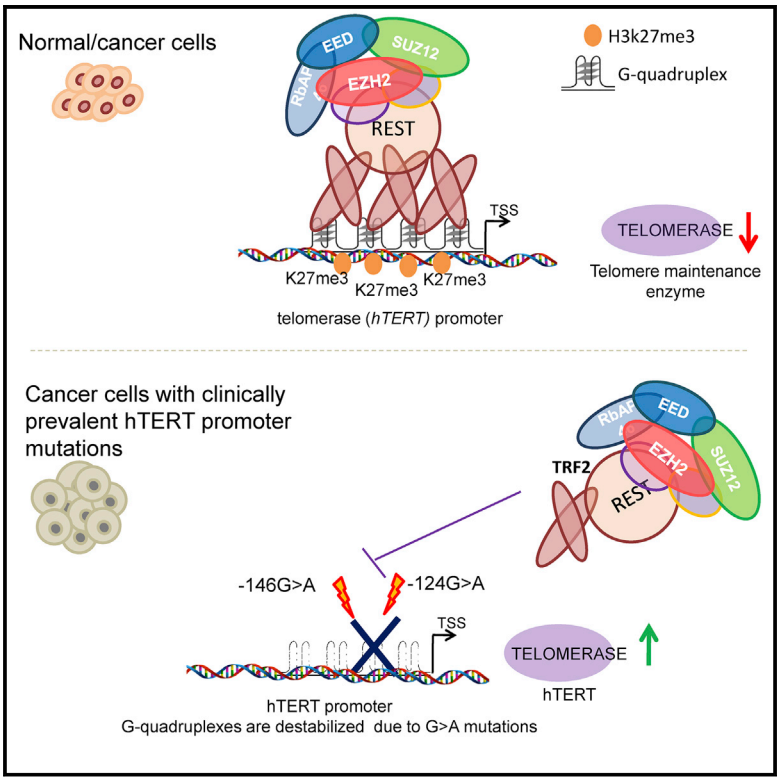

Highlights

- Non-telomeric TRF2 suppresses re-activated human telomerase in glioblastoma cells
- PRC2 recruitment depends on the TRF2 hTERT-G-quadruplex interaction
- Clinically deleterious *hTERT* promoter mutations disrupt G4-TRF2 association
- G4 stabilization reinstates TRF2-induced *hTERT* repression in patient glioblastoma

Authors

Shalu Sharma, Ananda Kishore Mukherjee, Shuvra Shekhar Roy, ..., Gaute Nesse, Deo Prakash Pandey, Shantanu Chowdhury

Correspondence

shantanuc@igib.in

In brief

Sharma et al. show transcriptional repression of *hTERT* by non-telomeric TRF2. TRF2 binds *hTERT* promoter G-quadruplex and recruits the REST/PRC2-complex. High-frequency clinical mutations associated with cancer destabilize *hTERT* promoter G-quadruplex, compromise TRF2 binding, and result in *hTERT* re-activation. Stabilization of G-quadruplex reinstates TRF2 binding and *hTERT* re-suppression in patient-derived glioblastoma cells.

Sharma et al., 2021, Cell Reports *35*, 109154
May 18, 2021
https://doi.org/10.1016/j.celrep.2021.109154

CellPress

Cell Reports

CellPress
OPEN ACCESS

Article

Human telomerase is directly regulated by non-telomeric TRF2-G-quadruplex interaction

Shalu Sharma,[1,2,7,8] Ananda Kishore Mukherjee,[1,2,7,8] Shuvra Shekhar Roy,[1,2,7] Sulochana Bagri,[1,2,7] Silje Lier,[5,6] Meenakshi Verma,[1,7] Antara Sengupta,[1,2,7] Manish Kumar,[4,7] Gaute Nesse,[5] Deo Prakash Pandey,[5] and Shantanu Chowdhury[1,2,3,7,9,*]

[1]Integrative and Functional Biology Unit, CSIR-Institute of Genomics and Integrative Biology, New Delhi 110025, India
[2]Academy of Scientific and Innovative Research (AcSIR), Ghaziabad 201002, India
[3]GNR Knowledge Centre for Genome and Informatics, CSIR-Institute of Genomics and Integrative Biology, New Delhi 110025, India
[4]Imaging Facility, CSIR-Institute of Genomics and Integrative Biology, New Delhi 110025, India
[5]Department of Microbiology, Oslo University Hospital, Oslo, Norway
[6]Institute of Basic Medical Sciences, University of Oslo, Oslo, Norway
[7]CSIR-Institute of Genomics and Integrative Biology, New Delhi 110025, India
[8]These authors contributed equally
[9]Lead contact
*Correspondence: shantanuc@igib.in
https://doi.org/10.1016/j.celrep.2021.109154

SUMMARY

Human telomerase reverse transcriptase (*hTERT*) remains suppressed in most normal somatic cells. Resulting erosion of telomeres leads eventually to replicative senescence. Reactivation of *hTERT* maintains telomeres and triggers progression of >90% of cancers. However, any direct causal link between telomeres and telomerase regulation remains unclear. Here, we show that the telomere-repeat-binding-factor 2 (TRF2) binds *hTERT* promoter G-quadruplexes and recruits the polycomb-repressor EZH2/PRC2 complex. This is causal for H3K27 trimethylation at the *hTERT* promoter and represses *hTERT* in cancer as well as normal cells. Two highly recurrent *hTERT* promoter mutations found in many cancers, including ~83% glioblastoma multiforme, that are known to destabilize *hTERT* promoter G-quadruplexes, showed loss of TRF2 binding in patient-derived primary glioblastoma multiforme cells. Ligand-induced G-quadruplex stabilization restored TRF2 binding, H3K27-trimethylation, and *hTERT* re-suppression. These results uncover a mechanism of *hTERT* regulation through a telomeric factor, implicating telomere-telomerase molecular links important in neoplastic transformation, aging, and regenerative therapy.

INTRODUCTION

Telomeres are nucleoprotein complexes that protect chromosome ends. In humans, the reverse transcriptase subunit (*hTERT*) of telomerase, necessary for telomere synthesis, is repressed in most adult somatic cells (Blackburn et al., 2006; Cech, 2004; Cong et al., 2002; Shay and Wright, 2019). Loss of *hTERT* repression resulting in increased telomerase activity is instrumental for telomere maintenance, which aids cancer initiation and progression in >90% of human cancers (Artandi and DePinho, 2010; Cao et al., 2002; Pandita et al., 2015; Shay and Bacchetti, 1997). Although these suggest direct molecular links between *hTERT* regulation and telomeres—possibly through telomeric factors—this remains unclear.

Recent work by us and others show non-telomeric DNA binding of telomeric proteins telomere-repeat-binding-factor 1 (TRF1), telomere-repeat-binding-factor 2 (TRF2), and RAP1 (Martinez et al., 2010; Mukherjee et al., 2018, 2019a; Paeschke et al., 2005; Sarthy et al., 2009; Simonet et al., 2011; Yang et al., 2011). We found ~20,000 TRF2 binding sites genome-wide, a large fraction of which comprised non-duplex structures called G-quadruplexes (Mukherjee et al., 2019a). Binding of TRF2 to DNA secondary structures including DNA and RNA G-quadruplexes were implicated in multiple studies (Baker et al., 2009; Benarroch-Popivker et al., 2016; Biffi et al., 2012; Fouché et al., 2006; Islam et al., 2014; Mishra et al., 2016; Pedroso et al., 2009; Purohit et al., 2018; Rhodes and Lipps, 2015). Furthermore, other telomere-binding proteins like heterochromatin protein 1 (HP1)-alpha, TIN2, and POT1, were found to interact with G-quadruplexes (Baumann and Price, 2010; Chow et al., 2018; Pike et al., 2019; Roach et al., 2020; Smogorzewska et al., 2000; Zaug et al., 2005). Because the *hTERT* promoter harbors multiple G-quadruplex-forming sequences (Li et al., 2017; Lim et al., 2010; Monsen et al., 2020; Palumbo et al., 2009; Saha et al., 2017; Yu et al., 2012), we asked whether TRF2 associates with the *hTERT* promoter and if this affects *hTERT* regulation.

Two somatic *hTERT* promoter mutations (G > A at the -124^{th} or -146^{th} bp from the translation start site), highly recurrent in multiple cancers including glioblastoma multiforme (GBM) (>80%), melanomas (>70%), hepatocellular (>40%), and

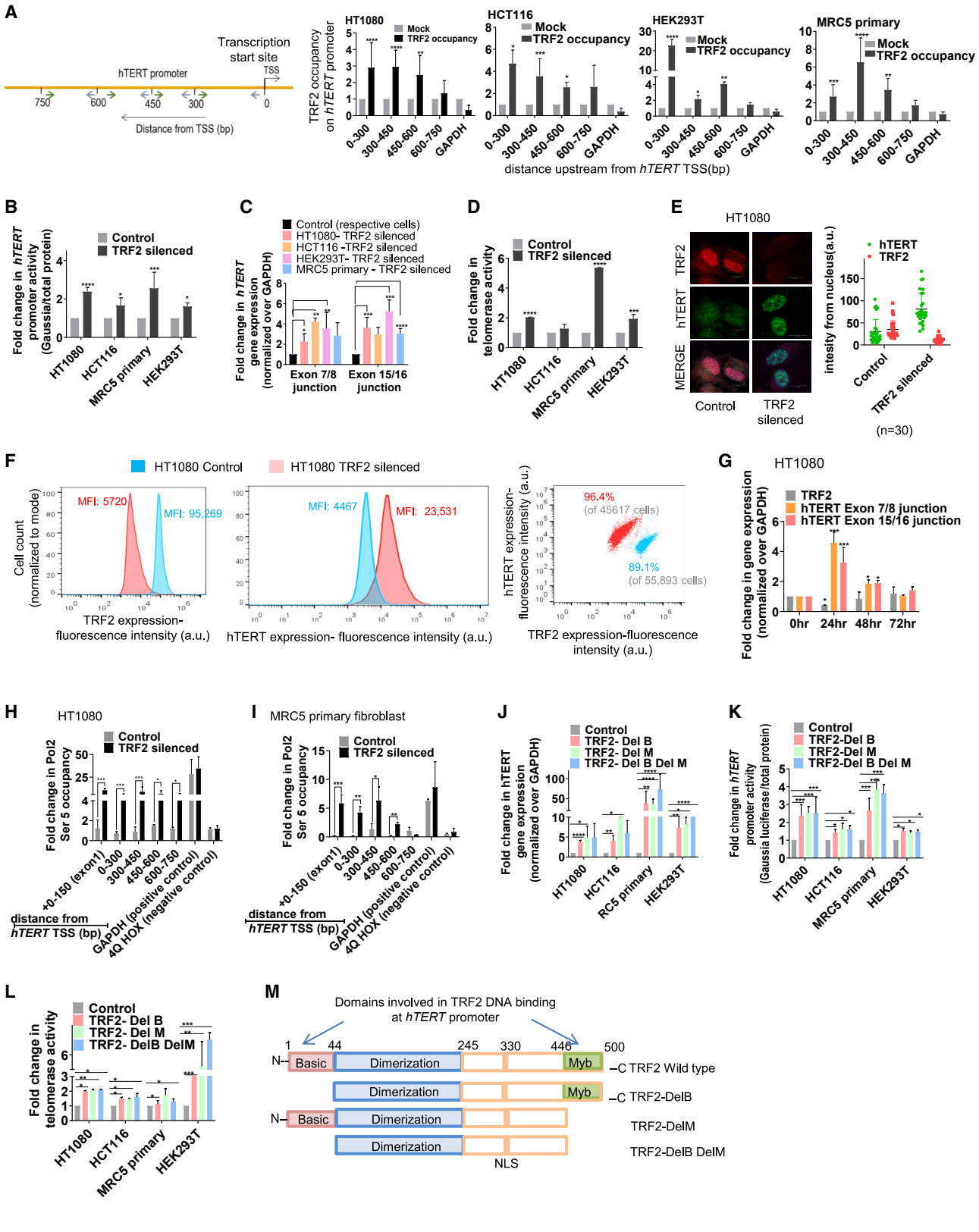

(legend on next page)

urothelial bladder (>50%) carcinomas, induce *hTERT* reactivation (Horn et al., 2013; Huang et al., 2013; Killela et al., 2013; Liu et al., 2016). Both mutations are within G-quadruplex-forming sequences and destabilized G-quadruplex in solution (Kang et al., 2016). Here, we show these mutations disrupt TRF2 interaction with *hTERT* promoter G-quadruplexes. As a result, TRF2-induced suppression of *hTERT* was lost in glioblastoma patient-derived cells, melanoma, and hepatocellular carcinoma cells. In the presence of G-quadruplexes stabilizing ligands, TRF2 binding was regained, re-suppressing telomerase across cells harboring *hTERT* promoter mutations.

RESULTS

TRF2 directly binds the *hTERT* promoter and regulates *hTERT* expression and telomerase activity in cancer and normal cells

Reads from TRF2 chromatin immunoprecipitation sequencing (ChIP-seq) peaks (recently reported by us) (Mukherjee et al., 2019a) mapped to the *hTERT* promoter (Figure S1A). TRF2 binding on the *hTERT* promoter spanned from the transcription start site (TSS) up to ~600 bp upstream in human cancer (fibrosarcoma HT1080 and colon HCT116 cells) as well as normal (MRC5 primary fibroblasts) and immortalized (embryonic kidney HEK293T) cells (Figure 1A). Normal somatic cells are known to have low telomerase activity. We also noted this on comparing *hTERT* expression and telomerase activity across the four cell types (Figures S1B and S1C). On finding TRF2 occupancy at the *hTERT* promoter in the non-cancer cell types as well, we studied the role of TRF2 in telomerase regulation in both normal and cancer cells.

hTERT promoter activity (from +33 to −1,267 bp promoter-luciferase reporter construct in plasmid) was enhanced on small interfering RNA (siRNA)-mediated TRF2 silencing in all the four cell types (Figure 1B). Silencing of TRF2 upregulated *hTERT* expression (both the reverse transcriptase [exon 7/8] and the full-length [exon 15/16] transcripts) (Figure 1C) and telomerase activity across cell lines (Figure 1D).

Immunofluorescence (IF), following TRF2 silencing, revealed 2- to 3-fold enhanced hTERT within nucleus in HT1080 (Figure 1E). In fluorescence-activated cell sorting (FACS) on TRF2 silencing, the mean fluorescence intensity (MFI) of hTERT increased by ~5.2-fold relative to control (scrambled treated) cells (Figure 1F). TRF2 silencing experiments were performed using previously published TRF2 siRNA and confirmed using western blots (Figure S1D).

Further, to confirm direct impact of TRF2 on *hTERT* expression, TRF2 was first depleted using siRNA in HT1080 cells, which gave enhanced *hTERT* expression (see STAR Methods for details). Thereafter, cells were maintained for 72 h with no further siRNA addition when TRF2 levels gradually increased—concomitant decline in *hTERT* was evident (Figure 1G). As expected, Pol-II (initiation RNA polymerase phospho-Ser5) occupancy increased significantly at the *hTERT* promoter, including exon 1 (0 to +150 bp from TSS), following TRF2 silencing in both HT1080 and MRC5 cells (Figures 1H and 1I). Taken together, these results suggested transcriptional control of functional *hTERT* by TRF2. The antibody used for hTERT was confirmed by FACS and IF in super-telomerase cells that constitutively overexpress telomerase (characterized earlier) (Cristofari and Lingner, 2006) (Figure S1E).

Both MYB and basic domains of TRF2 are necessary for transcription regulation of *hTERT*

Overexpression of FLAG-tagged TRF2-DelM (lacking C-terminal-Myb [M] domain), TRF2-DelB (lacking N-terminal-basic [B] domain), or TRF2-DelB-DelM (lacking both B and M domains) mutants gave enhanced expression of the *hTERT* full-transcript

Figure 1. TRF2 binds at the *hTERT* promoter and transcriptionally represses *hTERT*

(A) Scheme showing the *hTERT* promoter with position of primers designed for ChIP-qPCR (quantitative real-time PCR from ChIP DNA) (indicated by arrows) spanning from 0 to −750 bp of TSS, TRF2 ChIP followed by *hTERT* promoter-spanning qPCR for TRF2 binding in cancer (HT1080 and HCT116), and MRC5 and HEK293T cells relative to immunoglobulin G (IgG) ChIP (Mock) (see STAR Methods for detail on ChIP DNA qPCR data analysis).

(B) Effect of siRNA-induced TRF2 silencing on *hTERT* promoter activity in cells 48 h after transfection; +33 to −1,267 bp *hTERT* promoter cloned upstream of *Gaussia* luciferase. Cells treated with scrambled siRNA as control.

(C) Effect of TRF2 silencing on *hTERT* expression; functional (exon 7/8) and full (exon 15/16) transcripts. Fold change normalized over respective cells treated with scrambled siRNA control.

(D) Effect of TRF2 silencing on telomerase activity quantified using telomerase-repeat-amplification-protocol (TRAP) followed by ELISA (see STAR Methods); signal normalized over scrambled treated cells (control). HCT116 cells had relatively high telomerase activity in control than other cells, and the increase following TRF2-silencing was modest.

(E) Immunofluorescence staining of hTERT and TRF2 protein in HT1080 cells. TRF2 and hTERT were stained using Alexa fluor-594 (red signal) and Alexa fluor-498 (green signal), respectively. Quantification of nuclear signal (marked by DAPI, blue) from 30 cells (n = 30) shown in respective right panels.

(F) Flow cytometry using dual staining for hTERT and TRF2 in HT1080 control (scrambled siRNA-treated) and TRF2-silenced cells. Mean intensity of fluorescence (MIF) for hTERT and TRF2 is shown (left and center panel); right panel shows total cell populations monitored: 89.1% of 55,893 cells were analyzed (gated) for control (scrambled treated) cells (with higher TRF2 and relatively low hTERT); 96.4% of 45,617 cells were analyzed for TRF2-silenced cells (lower TRF2 and relatively high hTERT). The cell counts were normalized to respective modes for comparative representation in the left and center panels.

(G) Expression of *TRF2* and *hTERT* (exon7/8 and exon15/16) 24, 48, and 72 h following TRF2 siRNA treatment in HT1080 cells. The siRNA complex was removed 6 h after initial transfection.

(H and I) Pol2 (Ser5) occupancy spanning *hTERT* promoter following TRF2 silencing in HT1080 (H) and MRC5 cells (I). Cells treated with scrambled siRNA as control.

(J–L) Expression of the full-length *hTERT* transcript (exon 15/16) (J) and *hTERT* promoter activity (K) and telomerase activity (L) following expression of TRF2 deletion mutants. Results were normalized to untransfected control cells in each case.

(M) Scheme showing the full-length and mutant forms of TRF2 used in the study.

All error bars represent ± SDs from mean. p values calculated by paired/unpaired t test and two-way ANOVA in (G) and (J)–(L) (*$p < 0.05$, **$p < 0.01$, ***$p < 0.005$, ****$p < 0.0001$).

(Figure 1J), enhanced promoter (Figure 1K), and telomerase activity (Figure 1L) in HT1080, HCT116, MRC5, and HEK293T cells (scheme comparing TRF2 deletion mutants with wild-type TRF2 shown in Figure 1M; dimerization domain was common in all). ChIP with anti-FLAG antibody following expression of the FLAG-tag-TRF2 deletion mutants in HT1080 cells did not show occupancy of TRF2-DelM, TRF2-DelB, or TRF2-DelB-DelM at the *hTERT* promoter (Figure S1F). Expression of the deletion mutants was confirmed in each case using anti-FLAG antibody (Figure S1G).

Further, occupancy of the full-length endogenous TRF2 at the *hTERT* promoter was significantly reduced following expression of TRF2-DelB, DelM, or DelB-DelM mutants (Figure S1H). The TRF2 antibody recognized the full-length endogenous TRF2 as well as the TRF2-deletion mutants (Figure S1I). Therefore, in the absence of any binding of the TRF2 deletion mutants at the *hTERT* promoter (as shown above (Figure S1F), the reduced TRF2 ChIP is likely to result from lack of endogenous full-length TRF2 occupancy on expressing TRF2-deletion mutants.

We next checked the effect of the TRF2-deletion mutants on *hTERT* repression. All the three TRF2-deletion mutants (TRF2-DelB, DelM, or DelB-DelM) induced *hTERT* promoter activity, whereas full-length TRF2 expression did not affect *hTERT* promoter activity significantly (Figure S1J). Expression of the FLAG-tagged full-length TRF2 or the respective TRF2 deletion mutants was confirmed using anti-FLAG antibody (Figure S1K). Together, these findings show that both the N-terminal B domain and the C-terminal M domain of TRF2 are required for *hTERT* repression.

Epigenetic state of chromatin at the *hTERT* promoter is TRF2-dependent

TRF2-mediated promoter histone methylation was observed earlier (Benetti et al., 2008; Mukherjee et al., 2018, 2019a; Ye et al., 2014). Here, we checked histone-activation (H3K4me1 and H3K4me3) and repressor (H3K27me3 and H3K9me3) marks at the *hTERT* promoter following TRF2 silencing. ChIP-qPCR for the four histone marks spanning 750 bp upstream of *hTERT* TSS (as in Figure 1A) showed significant loss of the H3K27me3 repressor in both HT1080 and MRC5 cells (Figures 2A and 2B); H3K4me1, H3K4me3, or H3K9me3 did not change significantly on TRF2 silencing (Figures S2A and S2B).

Recruitment of the polycomb repressor complex (PRC2) at the *hTERT* promoter induced by TRF2

The EZH2 subunit of the polycomb-repressor-complex-2 (PRC2) catalyzes histone H3K27 trimethylation resulting in gene inactivation (Margueron and Reinberg, 2011; Stern et al., 2017). In both HT1080 and MRC5 cells, TRF2 silencing resulted in loss of EZH2 occupancy at the *hTERT* promoter (Figures 2C and 2D). However, silencing of EZH2 did not affect TRF2 occupancy (Figure S2C) suggesting TRF2-induced recruitment of EZH2/PRC2 at the *hTERT* promoter.

Recruitment of PRC2 by the RE1-silencing-factor (REST) (Dietrich et al., 2012; McGann et al., 2014) and REST-dependent gene silencing has been reported (Bruce et al., 2004). Further, interaction of REST with TRF2 was reported (Mukherjee et al., 2018, 2019a; Zhang et al., 2011). Here, we tested if TRF2 recruited REST to the *hTERT* promoter. TRF2 silencing, in HT1080 and MRC5 cells, gave reduced REST association at the *hTERT* promoter (spanning 750 bp) showing TRF2-dependent REST occupancy (Figures 2E and 2F). This was supported by intracellular TRF2-REST interaction in HT1080 cells (Hussain et al., 2017) and in MRC5 cells shown here using co-immunoprecipitation (coIP) of REST with anti-TRF2 antibody (Figure S2D).

TRF2 silencing resulted in loss of REST occupancy (Figures 2E and 2F) whereas REST silencing did not reduce TRF2 binding at the *hTERT* promoter (Figure S2E). Further, REST-reChIP, from the TRF2-ChIP fraction, in HT1080 and MRC5 cells confirmed TRF2- REST association at the *hTERT* promoter (Figures 2G and 2H). The *synapsin* promoter reported for REST binding, but not TRF2 (Mukherjee et al., 2018, 2019a), was used as control: REST-reChIP as expected was negative for the *synapsin* promoter. Reverse of this, i.e., TRF2-reChIP following immunoprecipitation with anti-REST antibody confirmed TRF2-REST co-binding (Figure S2F). TRF2-reChIP was negative for the *synapsin* promoter as expected.

Overexpression of the TRF2-delB or TRF2-delM deletion mutants resulted in loss of REST occupancy from the *hTERT* promoter (Figure S2G); whereas REST occupancy at the *synapsin* promoter (where REST and TRF2 do not interact) remained unaffected. Together, these showed full-length TRF2 binding at the *hTERT* promoter is required to engage the EZH2/PRC2-REST repressor complex. This is causal for the H3K27me3 modification inducing restrictive chromatin, which suppressed *hTERT* expression.

CoIP of TRF2 with REST was clear (Figure S2D). As reported earlier (Dietrich et al., 2012), we confirmed coIP of REST with EZH2 (Figure S2H). However, coIP of EZH2 with TRF2 was not evident (data not shown). Therefore, it is likely that TRF2 recruits REST and EZH2 association is through REST, suggesting a multi-protein complex where direct TRF2-EZH2 binding is relatively weak for detection by coIP.

TRF2 association at the *hTERT* promoter is independent of telomeres

We inserted a *hTERT* promoter *Gaussia* luciferase reporter at the CCR5 safe-harbor locus, 46 Mb away from the nearest telomere, by CRISIP/Cas9-mediated editing in HEK293T cells (Figure 3A). Luciferase expression from the reporter was enhanced on silencing TRF2 or on overexpression of the TRF2 deletion mutants, whereas overexpression of full-length TRF2 had no significant effect on *hTERT* expression (Figure 3B). TRF2 binding at the inserted *hTERT* promoter was clearly observed (Figure 3C). ChIP-qPCR was performed using primers specific to the inserted loci (+113 to −196 bp of TSS, indicated in Figure 3A).

We reasoned interaction with telomeres by looping (Kim et al., 2016) would show presence of the shelterin factors POT1, TRF1, and RAP1, along with TRF2, at the inserted promoter (at the CCR5 locus) in HEK293T cells. In contrast to TRF2, binding of the other shelterins POT1, TRF1, or RAP1 was not found (Figure 3D). However, occupancy of POT1, TRF1, or RAP1 was observed ~100 kb downstream of the *hTERT* locus reported to engage telomeres (Kim et al., 2016), which we used as positive control. Telomeric binding of POT1, TRF1, RAP1, and TRF2 was confirmed independently using telomere-specific ChIP-PCR

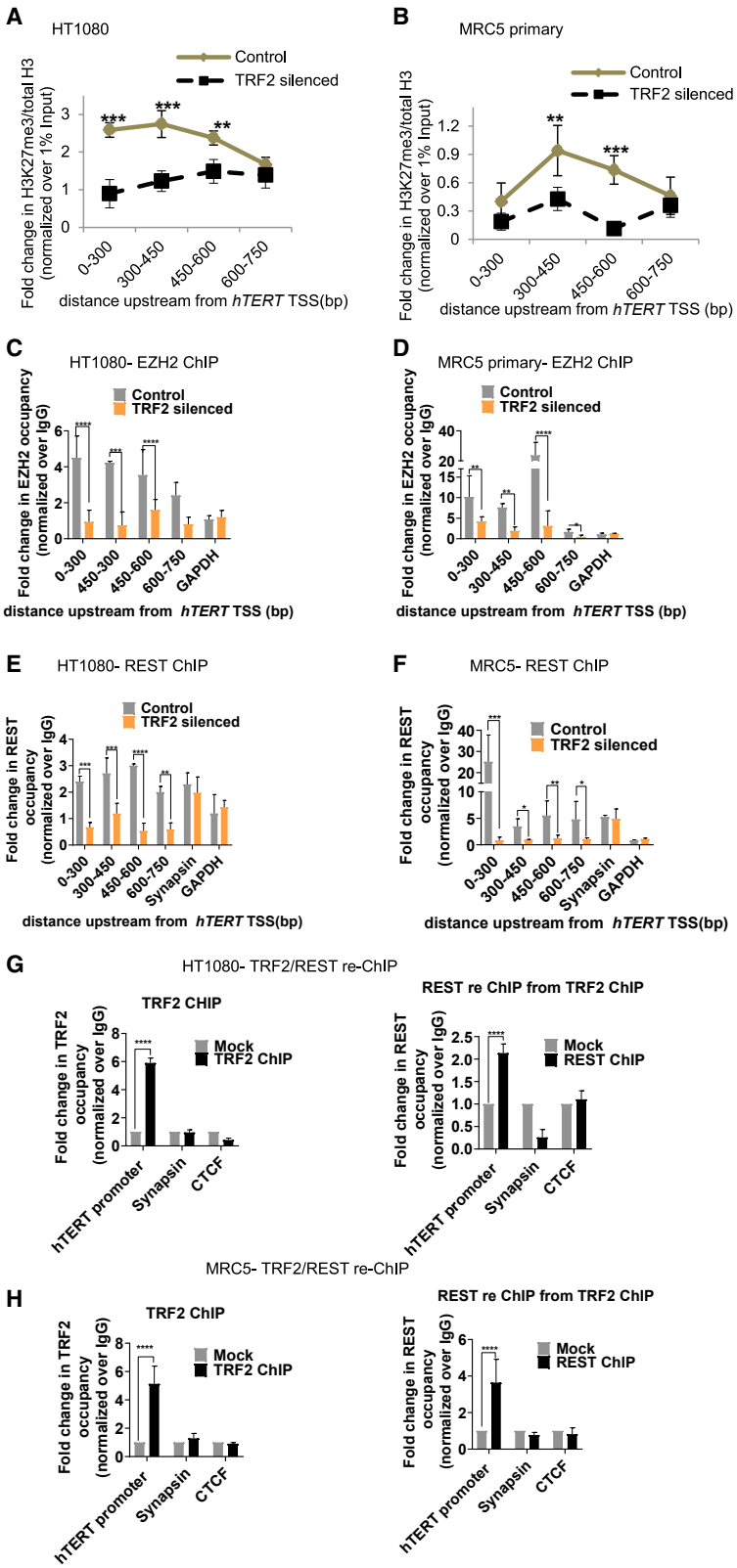

Figure 2. TRF2 recruits the polycomb repressor complex (PRC2) at the *hTERT* promoter

(A and B) Effect of TRF2 silencing on H3K27me3 occupancy (ChIP-qPCR) spanning 0–750 bp of the *hTERT* promoter HT1080 (A) and MRC5 (B) cells. Fold change represented as H3K27me3 ChIP over total H3 ChIP, normalized to 1% input in respective cases (see STAR Methods for detail).

(C and D) EZH2 occupancy on the *hTERT* promoter (spanning 0–750 bp) on silencing TRF2 in HT1080 (C) and MRC5 cells (D). Scrambled siRNA-treated cells as control.

(E and F) REST occupancy on the *hTERT* promoter on silencing TRF2 in HT1080 (E) and MRC5 (F) cells. *Synapsin* promoter reported for REST binding was used as control forTRF2-independent REST occupancy. Scrambled siRNA-treated cells as control.

(G and H) TRF2 ChIP followed by REST re-ChIP: TRF2 ChIP (left panel) and REST re-ChIP (right panel) in HT1080 (G) and MRC5 (H) cells at the *hTERT* core promoter (+38 to −237 bp). Synapsin, where REST binding is independent of TRF2 used as control for TRF2-REST co-binding in TRF2/REST-re-ChIP. GAPDH across replicates was not detectable following reChIP therefore CTCF used as negative control for reChIP experiments. All error bars represent ± SDs from mean values; p values calculated by paired/unpaired t test, for (A)–(F) two-way ANOVA was used (*p < 0.05, **p < 0.01, ***p < 0.005, ****p < 0.0001).

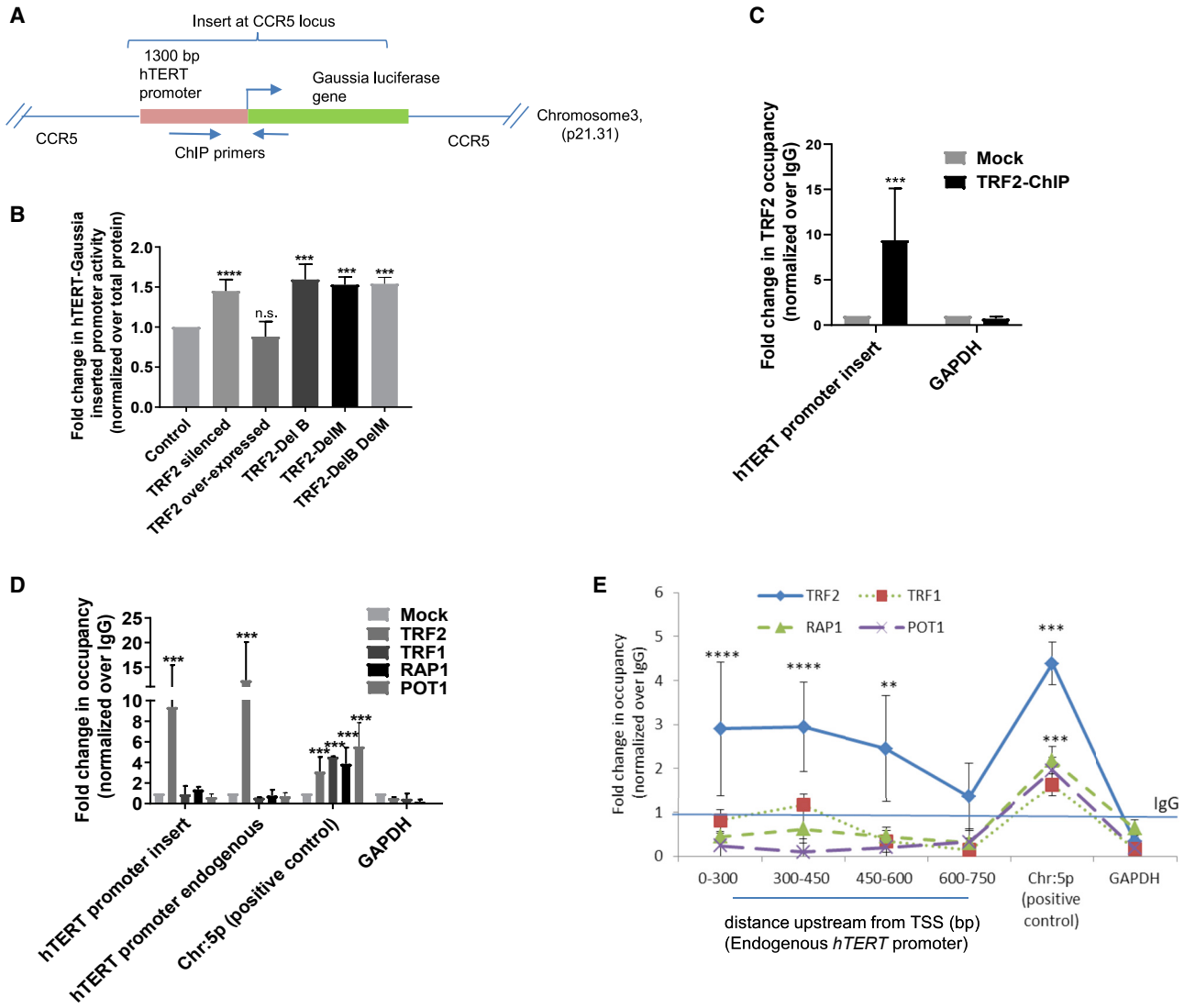

Figure 3. TRF2 binding on *hTERT* promoter is independent of telomeres

(A) Scheme showing insertion of *Gaussia* luciferase downstream of the *hTERT* promoter (+33 to −1,267 bp) at *CCR5* locus using CRISPR/Cas9-mediated editing in HEK293T cells (see Supplemental information for characterization of cells). Position of primers designed for ChIP-qPCR indicated by arrows.

(B) Effect of TRF2 silencing or expression of full-length TRF2 or TRF2-deletion mutants TRF2-DelB, TRF2-DelM, and TRF2-DelB-DelM on *hTERT*-promoter *Gaussia* luciferase activity relative to untreated control cells. Normalized using total protein in each case.

(C) qPCR following TRF2 ChIP at the inserted-*hTERT* promoter at CCR5 locus using primers shown in scheme above (A); normalized over mock (IgG). *GAPDH* promoter was used as negative control for TRF2 occupancy.

(D and E) qPCR following ChIP for TRF1, POT1, and RAP1: at the CCR5-locus-inserted-*hTERT* promoter and the endogenous *hTERT* promoter (+38 to −237 bp) in HEK293T cells (D) and spanning the endogenous *hTERT* promoter in HT1080 cells (E). Chromosome 5p region 100 kb downstream of the *hTERT* locus reported for physical association with telomeres by looping was used as positive control and GAPDH as negative control.

All error bars represent ± SDs from mean values; p values calculated by paired/unpaired t test; for (B), (D), and (E) two-way ANOVA was used (*$p < 0.05$, **$p < 0.01$, ***$p < 0.005$, ****$p < 0.0001$).

followed by dot-blot (Figure S3A; STAR Methods). Therefore, it is unlikely that the inserted *hTERT* promoter at the CCR5 locus (46 Mb away from telomeres) is bridged to the telomeres through looping interactions.

Next, we checked if TRF2 binding at the endogenous *hTERT* promoter was from telomeres through looping. Arguing as above, we tested occupancy of POT1, TRF1, and RAP1. Although TRF2 occupancy was clear (Figure 1A), we did not find POT1, TRF1, or RAP1 up to −750 bp of the endogenous *hTERT* promoter in HT1080 cells (Figure 3E); however, their binding in the region reported to engage telomeres by looping (Kim et al., 2016) was clear. Telomeric binding of POT1/TRF1/RAP1 was confirmed independently by ChIP-qPCR followed by dot-blot (Figure S3B; STAR Methods). Therefore, TRF2 association at the *hTERT* promoter was unlikely from telomere looping.

CellPress
OPEN ACCESS

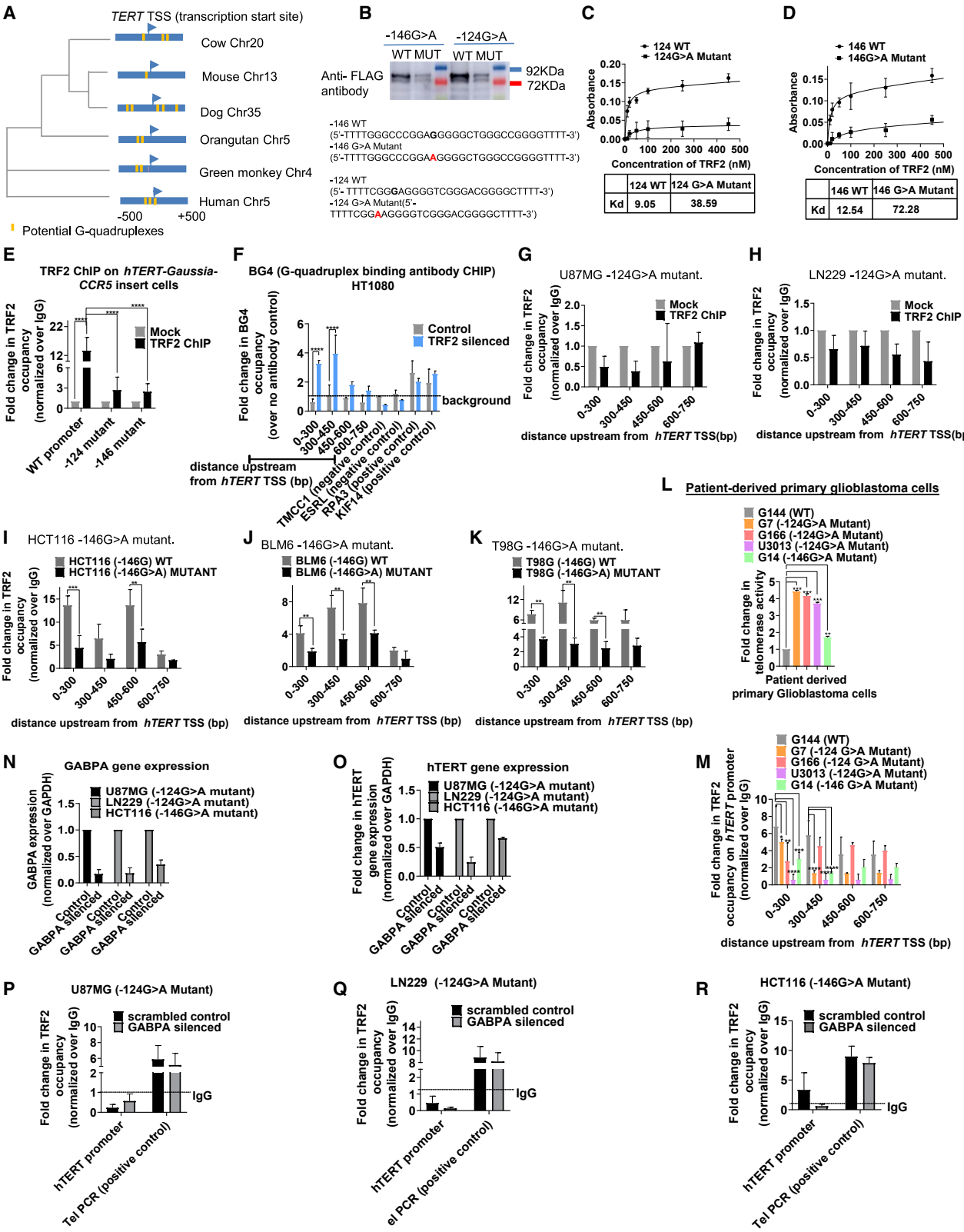

(legend on next page)

Although recruitment of RAP1 to TRF2 sites was noted earlier (Janoušková et al., 2015; Sarthy et al., 2009), we did not observe this in the case of the *hTERT* promoter. This is consistent with ChIP-seq showing that TRF2 and RAP1 binding is exclusive in a substantial number of sites suggesting all TRF2 binding sites may not recruit RAP1 (Yang et al., 2011).

TRF2 binding at the *hTERT* promoter was dependent on G-quadruplex

The *hTERT* promoter harbors an unusually high number of tandem G-quadruplex-forming sequences (31–35, 41) (Figure S4A). This is evolutionarily conserved, because other vertebrates also have putative G-quadruplexes within 500 bp of *TERT* TSS (Figure 4A). Interaction of TRF2 with G-quadruplex was reported by others and us (Biffi et al., 2012; Islam et al., 2014; Mishra et al., 2016; Mukherjee et al., 2019a; Pedroso et al., 2009; Purohit et al., 2018; Rhodes and Lipps, 2015). Here, we selected two *hTERT* promoter G-quadruplex-forming tracts (Figures S4A and S4B). The two tracts harbored the mutations (−124 bp (G > A) and −146 bp (G > A) (Figure S4A) frequently found in cancers, including GBM (Horn et al., 2013; Huang et al., 2013; Killela et al., 2013; Liu et al., 2016), that destabilized the G-quadruplexes *in vitro* (Kang et al., 2016) (Figure S4B).

To test interaction of TRF2 with *hTERT*-promoter G-quadruplex, flag-tagged TRF2 was expressed in HT1080 cells. Lysate from the cells was incubated with biotinylated wild-type or mutant (−124G > A/−146G > A) oligonucleotides (after allowing G-quadruplex formation by the oligonucleotides; see STAR Methods) and pulled down using streptavidin beads. Using anti-flag-antibody we observed enhanced TRF2 interaction with wild-type relative to the mutant oligonucleotides (Figures 4B and S4C). ELISA with recombinant TRF2 showed ∼4- to 6-fold higher affinity for the *hTERT* promoter G-quadruplex(es) relative to the respective mutant oligonucleotide(s) that destabilized the G-quadruplex (Figures 4C and 4D).

Next, we used the *hTERT* promoter *Gaussia* luciferase reporter at the CCR5 locus (Figure 3A). G > A substitutions were introduced either at the -124^{th} or the -146^{th} positions from translation start site of *hTERT*. TRF2 occupancy at the inserted *hTERT* promoter was significantly depleted for both the substitutions relative to the unsubstituted promoter (Figure 4E). As expected, TRF2 occupancy at the endogenous *hTERT* promoter remained unaltered in these cells (Figure S4D).

Although sequence tracts at the *hTERT* promoter that form G-quadruplexes in solution were shown, *in vivo* evidence for G-quadruplex formation has not been reported. We directly tested for *in vivo* presence of G-quadruplex at the endogenous *hTERT* promoter by ChIP using the reported G-quadruplex-binding antibody BG4 (Hänsel-Hertsch et al., 2018). Surprisingly, BG4 occupancy at the *hTERT* promoter was not detectable (Figure 4F). This could be because the G-quadruplexes were bound by protein(s) that restrict BG4 binding, as mentioned by authors earlier (Hänsel-Hertsch et al., 2018). Therefore, we tested BG4 binding after silencing TRF2. In cells lacking TRF2, occupancy of BG4 on the *hTERT* promoter was evident (Figure 4F).

The conformation of the *hTERT* promoter G-quadruplex remained intact in presence of recombinant purified TRF2 (Figure S4E). Ligands that stabilize G-quadruplex formation induced TRF2 binding whereas mutations that destabilized G-quadruplexes showed reduced/loss in TRF2 occupancy (described below). Further, multiple groups, including earlier work by us, show TRF2 binds/supports G-quadruplex formation (Biffi et al., 2012; Hussain et al., 2017; Mishra et al., 2016; Mukherjee et al., 2019a; Pedroso et al., 2009; Purohit et al., 2018; Rhodes and Lipps, 2015; Traczyk et al., 2020). Therefore, it is unlikely that TRF2 adversely affected G-quadruplex formation at the

Figure 4. TRF2-induced repression of *hTERT* is G-quadruplex-dependent

(A) Phylogenetic tree based on the sequence spanning ±500 bp of the *TERT* TSS across vertebrates. Presence and position of putative G-quadruplexes (configuration: stem of three Gs and loop size up to 15 bases) in respective organisms is shown in yellow.

(B) Oligonucleotide pull-down from cell lysate of HT1080 cells expressing FLAG-tagged TRF2; 5′-biotin-tagged oligonucleotides from *hTERT* wild-type (WT) or with mutations (MUT) at the -124^{th} or -146^{th} position were used for pull-down followed by western blot and probed using anti-FLAG antibody. Sequence of respective WT or MUT (base substitution shown in red), with TTTT overhangs to minimize steric interactions because of biotin or on ELISA plate (C and D below) given in the bottom panel.

(C and D) ELISA experiments using biotin-tagged *hTERT* promoter oligonucleotides for WT and the corresponding G > A mutation and increasing concentrations of purified TRF2 protein, WT with −124G > A mutant (C), and WT with corresponding 146G > A mutation (D). Significance for each point was calculated by paired t test, p value across all was $p < 0.0001$ in both (C) and (D).

(E) qPCR following TRF2 ChIP at the exogenously inserted WT or with −124/-146G > A mutation, *hTERT* promoter at the CCR5 locus in HEK293T cells relative to IgG (Mock). Scheme of the inserted *hTERT* promoter with ChIP-qPCR primer positions as in Figure 3A.

(F) qPCR following BG4 ChIP at the *hTERT* promoter spanning up to 750 bp upstream of TSS: fold-change in BG4 occupancy over experiment using no-antibody control (as per manufacturer's protocol) shown in TRF2-silenced or scrambled siRNA-treated HT1080 cells (control). Positive and negative controls for BG4 antibody were used as reported earlier.

(G and H) TRF2 ChIP-qPCR spanning 0–750 bp upstream of the *hTERT* promoter in glioblastoma U87MG (G) and LN229 (H) cell lines with −124G > A promoter mutation relative to IgG ChIP (Mock).

(I–K) TRF2 ChIP-qPCR spanning the *hTERT* promoter in cancer cell lines with or without the −146G > A promoter mutation: HCT116 cells (I), BLM6 cells (J), or T98G cells (K). Normalized over respective IgG ChIPs (see STAR Methods for details on data analysis). Single base substitutions were made in each case using CRISPR/Cas9-mediated editing.

(L and M) Telomerase activity quantified by ELISA TRAP (see STAR Methods) (L) and TRF2 ChIP-qPCR spanning the *hTERT* promoter in patient-derived primary glioblastoma cells (M): G144 (wild-type *hTERT* promoter); G7, G166, U3013 (−124G > A mutant *hTERT* promoter); and G4 (−146G > A mutant *hTERT* promoter).

(N and O) GABPA (N) and *hTERT* (O) gene expression following GABPA silencing using qRT-PCR relative to scrambled siRNA control.

(P–R) TRF2 ChIP followed by ChIP-qPCR for TRF2 occupancy at the *hTERT* mutant promoter following GABPA silencing in U87MG −124G > A mutant (P), LN229 −124G > A mutant (Q), or HCT116 −146G > A (R) mutant cells.

All error bars represent ± SDs from mean values. p values calculated by paired/unpaired t test, for (C)–(F), (L), and (M) two-way ANOVA was used (*$p < 0.05$, **$p < 0.01$, ***$p < 0.005$, ****$p < 0.0001$).

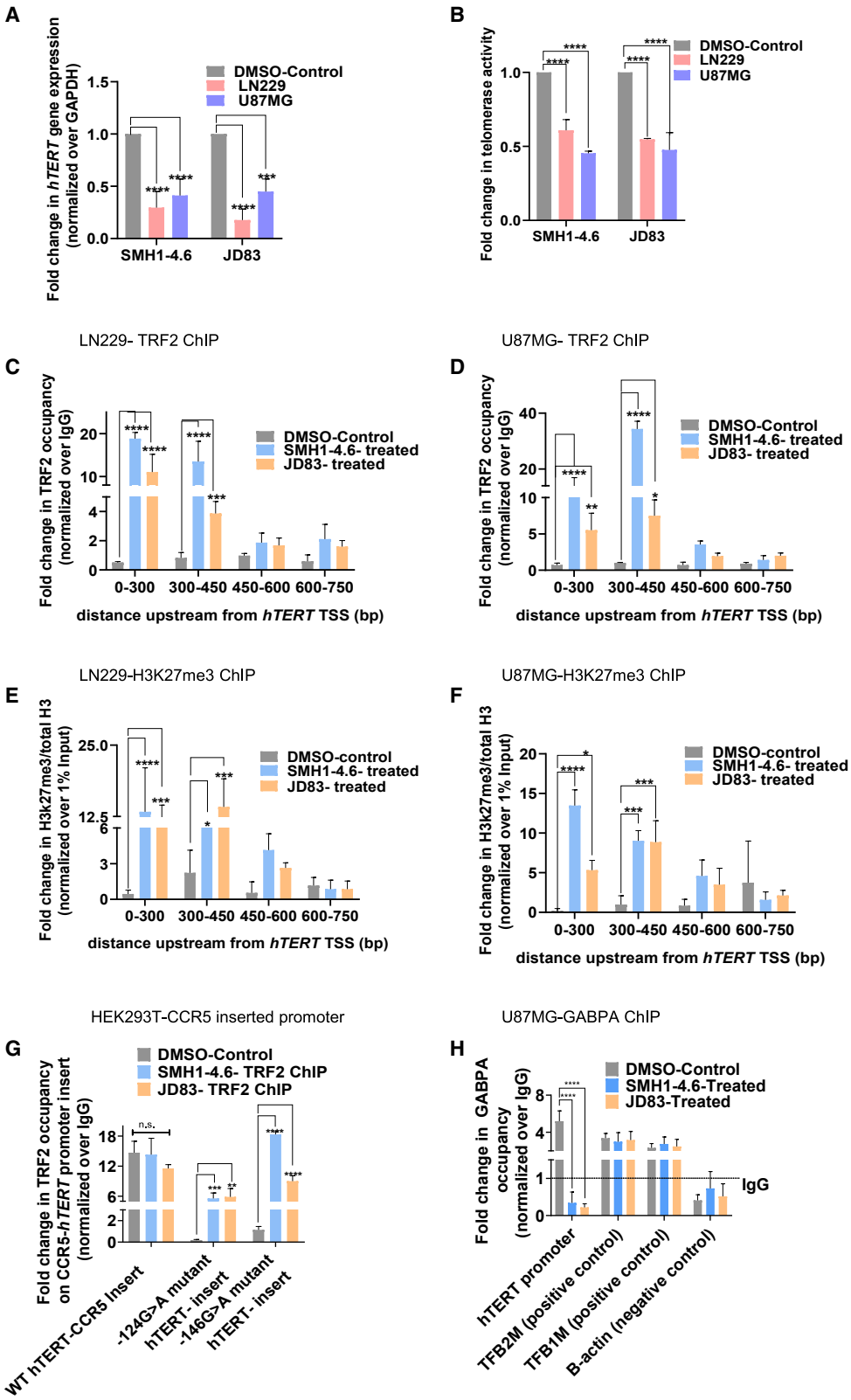

(legend on next page)

hTERT promoter excluding BG4 binding. Together, these results support *in vivo* G-quadruplex-dependent TRF2 binding at the *hTERT* promoter.

TRF2 occupancy is lost in cancers with *hTERT* promoter mutations

Two GBM cell lines, U87MG and LN229, both carrying endogenous −124G > A *hTERT* promoter mutation (Patil et al., 2015), were tested first. TRF2 binding up to −750 bp of the *hTERT* promoter was not detectable in both cell types (Figures 4G and 4H). Moreover, TRF2 overexpression did not result in TRF2 binding at the *hTERT* promoter in U87MG or LN229 (Figure S4F).

For the −146G > A *hTERT* promoter mutation, we tested three pairs of cancer cell lines with/without the mutation (a gift from the Tergaonkar laboratory; characterized earlier) (Akıncılar et al., 2016). In HCT116 colon cancer cells, the −146G > A mutation was introduced resulting in telomerase activation as expected (Akıncılar et al., 2016). In BLM6 melanoma and T98G GBM cells, −146G > A was corrected by A > G substitution, which gave telomerase repression (Akıncılar et al., 2016). In all the three cases, we found TRF2 occupancy was significantly reduced at the *hTERT* promoter with −146G > A mutation relative to the corresponding cell line without this change (Figures 4I–4K).

Loss/gain of H3K27me3 was TRF2-dependent (Figures 2A and 2B). Here, we checked HCT116 cells as a candidate case: loss of H3K27me3 modification from the *hTERT* promoter in cells with −146G > A mutation (as expected from loss of TRF2) was clearly observed relative to HCT116 cells without the mutation (Figure S4G). Loss of the H3K27me3 repressor mark in multiple cancer cell types with the *hTERT* promoter mutations has been reported (Akıncılar et al., 2016; Stern et al., 2017).

Next, we studied primary cells obtained from five grade 4 GBM patients. On sequencing the *hTERT* promoter (38 bp downstream to 237 bp upstream of ATG), we found three cases with −124G > A (G7, G166, and U3013), one case with −146G > A mutation (G14), and one case with no mutation (G144) (STAR Methods). Telomerase activity, as expected, was several-folds higher in GBM cells with either −124/−146 G > A mutation (G7, G166, U3013, or G14) compared to G144 with no *hTERT* promoter mutation (Figure 4L). TRF2 occupancy at the *hTERT* promoter was significantly reduced in G7, G166, U3013, and G14 relative to the G144 primary GBM case (Figure 4 M). Therefore, in different cancer cell types, including primary patient-derived GBM, TRF2 binding at the *hTERT* promoter was lost on G-quadruplex de-stabilization in case of −124/−146 G > A mutations.

The −124/-146G > A mutations create novel binding site(s) resulting in binding of the ETS factor GABPA at the *hTERT* promoter (Akıncılar et al., 2016; Bell et al., 2015; Stern et al., 2017). Therefore, it is possible that GABPA binding excludes/competes with TRF2 binding at the *hTERT* promoter with the mutation(s). To test this we checked for TRF2 occupancy at the *hTERT* promoter after silencing GABPA in the *hTERT* promoter mutant cell lines U87MG, LN229 (−124G > A mutant) and HCT116 (−146G > A mutant as described above) using previously published siRNA against GABPA (Stern et al., 2017). GABPA silencing was confirmed using qRT-PCR (Figure 4N); and *hTERT* expression was repressed on GABPA silencing as reported earlier (Akıncılar et al., 2016; Stern et al., 2017) (Figure 4O). We found that in absence of GABPA, TRF2 occupancy was not restored (*hTERT* core promoter +38 to −237 bp) across any of the three cell lines with *hTERT* promoter mutation(s) (Figures 4P–4R). Therefore, it is unlikely that TRF2 and GABPA compete for binding at the mutant *hTERT* promoter and further support loss of TRF2 because of de-stabilization of the promoters G-quadruplexes.

Stabilization of G-quadruplex using ligands reinstates TRF2 binding and re-suppresses activated telomerase

On observing loss of TRF2 binding in cells with *hTERT* promoter mutations that destabilized G-quadruplex formation, we next tested if stabilization of the G-quadruplex rescued TRF2 binding. Four reported intracellular G-quadruplex binding ligands (Figure S5A; Table S1) were screened using LN229 GBM cells (harboring −124G > A mutation) with reactivated telomerase. Two ligands, SMH1-4.6 and JD83, induced *hTERT* repression in LN229 cells (Figure 5A). SMH1-4.6 or JD83 treatment gave ~40%–50% repression of *hTERT* in U87MG cells (Figure 5A) and significant repression of telomerase activity in both U87MG and LN229 cells (Figure 5B). TRF2 expression remained relatively unaltered in presence of the ligands (Figure S5B).

On treatment with SMH1-4.6 or JD83, TRF2 binding at the *hTERT* promoter (up to 450 bp from TSS) increased significantly in both LN229 and U87MG cells (Figures 5C and 5D). On observing that the ligands SMH1-4.6 or JD83 restored TRF2 occupancy at the *hTERT* promoter, we tested their effect on the conformation of the mutant *hTERT* promoter sequence. In the presence of either SMH1-4.6 or JD83, the mutant oligonucleotides were restored to conformations similar to the wild-type G-quadruplex (Figure S5C). On the other hand, in presence of ligands 260697 or FC4ND08 that did not suppress *hTERT*

Figure 5. G-quadruplex-binding ligands re-suppress activated *hTERT* in glioblastoma multiforme with mutations in the *hTERT* promoter

(A and B) *hTERT* expression (A) and telomerase activity (B) in glioblastoma multiforme (GBM) cell lines U87MG and LN229 (with −124G > A *hTERT* promoter mutation) following treatment with G-quadruplex-binding ligands SMH1-4.6 and JD83 (2.5 μM) or DMSO for 24 h.

(C and D) TRF2 ChIP-qPCR spanning the *hTERT* promoter following treatment with SMH1-4.6 and JD83 (2.5 μM) or DMSO for 24 h in LN229 (C) or U87MG (D) cells.

(E and F) Fold change in repressor histone mark H3K27me3 by ChIP-qPCR spanning the *hTERT* promoter following treatment with SMH1-4.6 and JD83 (2.5 μM) or DMSO for 24 h in LN229 (E) or U87MG (F) cells. Fold-change shown with respect to total H3 ChIP; respective ChIPs were normalized to 1% input.

(G) TRF2 ChIP-qPCR at the exogenously inserted CCR5-locus-*hTERT* promoter with either the wild-type or −124G/−146G > A *hTERT* promoter mutations in HEK293T cells following treatment with SMH1-4.6 and JD83 (2.5 μM) or DMSO-treated (control) for 24 h. Normalized to IgG ChIP in each case.

(H) GABPA ChIP followed by qPCR at the *hTERT* core-promoter (+38 to −237 bp); in U87MG (−124G > A mutant) cells following treatment with SMH1-4.6 and JD83 (2.5 μM) or DMSO (control) for 24 h. Normalized to IgG in each case. TFB1M and TFB2M are positive control and B-actin is negative control for GABPA ChIP. All error bars represent ± SDs from mean values. p values calculated by paired/unpaired t test or two-way ANOVA (*p < 0.05, **p < 0.01, ***p < 0.005, ****p < 0.0001).

expression, the mutant *hTERT* promoter oligonucleotides did not regain the G-quadruplex conformation (Figure S5D). Unlike SMH1-4.6/JD83, in presence of the ligands 260697 or FC4ND08, TRF2 occupancy at the mutant *hTERT* promoter was not restored (Figures S5E and S5F). Further, we noted a gain in H3K27me3 repressor modification spanning the *hTERT* promoter in both cell lines on treatment with SMH1-4.6/JD83 (Figures 5E and 5F), consistent with TRF2-induced gain in H3K27me3 seen earlier (Figures 2A and 2B).

Next, we used the CCR5-locus *hTERT* promoter *Gaussia* luciferase reporter cell lines with/without the −124/−146 mutation. Treatment with SMH1-4.6 or JD83 resulted in a significant increase of TRF2 occupancy only at the inserted mutant *hTERT* promoter—and not at the wild-type *hTERT* promoter (Figure 5G).

GABPA is known to bind the *hTERT* mutant promoter (Akıncılar et al., 2016; Bell et al., 2015; Stern et al., 2017). Therefore, we next tested the effect of ligand-mediated promoter G-quadruplex stabilization on GABPA occupancy. Following treatment with SMH1-4.6 or JD83 in U87MG (−124G > A) mutant cells, we found significant loss in GABPA occupancy at the *hTERT* promoter (qPCR with *hTERT* promoter-spanning primers); GABPA occupancy at the positive controls (*TFB1M* and *TFB2M*) genes and negative control (*B-actin*) gene remained unaltered (Figure 5H). Together, these demonstrate ligand-mediated G-quadruplex stabilization results in recovery of promoter TRF2 occupancy, a gain in histone repressor H3K27me3, loss of GABPA binding, re-suppression of activated *hTERT*, and telomerase activity in cells with *hTERT* promoter mutations. These suggest that telomerase reactivation, frequently found in many cancers with −124/−146 *hTERT* promoter mutations, is likely due to loss of TRF2-induced repression of *hTERT*.

DISCUSSION

Here, we show TRF2-induced direct recruitment of the EZH2/PRC2-REST repressor complex at the *hTERT* promoter. This was causal for repressor histone modifications that maintained non-permissive chromatin at the *hTERT* promoter resulting in TRF2-mediated repression of *hTERT* expression and telomerase activity. A *hTERT* reporter, introduced using CRISPR/Cas9-mediated editing at the CCR5 locus, confirmed TRF2-induced repression of *hTERT* promoter activity. Using cells with/without specific mutations introduced at the endogenous *hTERT* promoter (using CRISPR/Cas9-mediated single-base editing) that disrupt the TRF2 binding site, we demonstrate direct TRF2 binding and transcriptional role of TRF2 in *hTERT* regulation.

TRF2 binding at the *hTERT* promoter was dependent on the stability of promoter G-quadruplex. Loss of TRF2 binding was observed in cells with *hTERT* promoter mutation(s) that destabilize G-quadruplex. The resulting decrease in repressor histone H3K27 trimethylation at the *hTERT* promoter and the enhanced *hTERT* expression was clear in all the cases we tested.

Depletion of hTERT functional protein was recently reported to induce telomere de-protection (Killedar et al., 2015; Tomlinson et al., 2015). This could also be independent of hTERT catalytic activity and result in growth arrest or apoptosis (Cesare et al., 2013; Perera et al., 2019; Sarthy and Baumann, 2010). G-quadruplex binding ligands have been previously reported to inhibit telomerase activity by targeting G-quadruplexes at telomeres (Balasubramanian et al., 2011; Bryan and Baumann, 2011; Granotier et al., 2005). Enrichment of the heterochromatin protein HP1-alpha at telomeres was recently noted to affect telomere structure and protection (Chow et al., 2018), possibly through association of HP1-alpha with G-quadruplex formed by telomeric DNA and RNA (transcribed from telomeres called telomeric repeat-containing RNA [TERRA]) (Roach et al., 2020; Smekalova and Baumann, 2013). POT1 independently, or in complex with shelterin proteins TIN2/TPP1, is essential for chromosome-end protection and telomerase processivity through disruption of telomeric G-quadruplexes (Bae and Baumann, 2007; Baumann and Price, 2010; Calvete et al., 2015; Pike et al., 2019; Zaug et al., 2005). Consistent with these findings, we observed growth arrest and cell death in GBM cells, on treatment with G-quadruplex binding ligands (data not shown). We note this could be through mechanisms, as mentioned above, in addition to hTERT depletion shown here. Further, sustained TRF2 depletion is known to induce telomeric DNA damage resulting in apoptosis and/or arrest in cell growth. In experiments where we silenced TRF2, this was transient, and experiments were conducted within 48 h of silencing. As expected, we did not detect any change in cell viability across cell lines.

Although transcriptional repression of *hTERT* by TRF2 has not been reported earlier, high TRF2 along with low hTERT levels was observed in CD4-T-lymphocytes and an osteosarcoma-derived cell line (El Maï et al., 2014; Escoffier et al., 2005). Smogorzewska et al. (2000), on the other hand, did not find any change in *hTERT* mRNA or promoter activity on TRF2 induction. In our hands, TRF2 silencing enhanced *hTERT* expression across cells; however, TRF2 overexpression did not alter *hTERT* expression significantly. It is therefore likely that chromatin at the *hTERT* promoter is constitutively repressed (with saturated levels of TRF2 occupancy), which is de-regulated on TRF2 downregulation. This is consistent with the observation showing that across 127 human tissues (NIH Epigenomics Roadmap), the region upstream of *hTERT* maintains a resting polycomb signature keeping it repressed—disruption of this signature results in telomerase activation (Valentijn et al., 2015).

Constitutive *hTERT* repression across normal tissue appears consistent with our observations from cells that are not derived from cancer—MRC5 and HEK293T cell lines. On finding TRF2 occupancy at the *hTERT* promoter in MRC5 and HEK293T cells, we asked whether, and if so how, TRF2 might affect *hTERT* regulation in non-cancer conditions. Although normal somatic cells are largely known to be devoid of telomerase expression and activity, we found basal expression of *hTERT* and telomerase activity as has been reported before in normal cells from multiple human tissues (Broccoli et al., 1995; Kyo et al., 1997; Masutomi et al., 2003; Wong et al., 2014). We observed downregulation of TRF2 and resulting loss of repressor histones promoted permissive chromatin changes and enhanced *hTERT* and telomerase activity. Further, Stern et al. (2017) recently showed EZH2/PRC2 binding on the *hTERT* core promoter across cancer cells. Adding to this and to work by others showing epigenetic regulation in cancer (Brien et al., 2016; Mukherjee et al., 2019b), we demonstrate TRF2 binding to be causal for recruitment of EZH2/PRC2 at the *hTERT* promoter. These results support the

role of TRF2 in maintaining the repressor polycomb signature at the *hTERT* promoter necessary for repressed *hTERT* and telomerase activity in normal conditions.

Promoter mutation(s) in *hTERT* was reported to generate site(s) for binding of the ETS transcription factor GABPA (Akıncılar et al., 2016; Bell et al., 2015; Li et al., 2015; Stern et al., 2017) leading to telomerase reactivation in cancer cells. We find the following aspects of interest in this context. First, GABPA silencing did not re-instate TRF2 binding (Figures 4P–4R). Second, ligand-induced stabilization of promoter G-quadruplex restored TRF2 occupancy at the mutant *hTERT* promoter (Figures 5C and 5D). Third, interestingly, GABPA binding at the mutant *hTERT* promoter was compromised on G-quadruplex stabilization (Figure 5H). Together, therefore, it is likely that GABPA binding (in case of mutations in the *hTERT* promoter) is facilitated by the permissive chromatin state due to destabilization of the G-quadruple and resultant loss of TRF2 and the PRC2 repressor complex.

Earlier, we reported TRF2 silencing resulted in altered H3K4me3 and H3K4me2 histone marks at the *p21* promoter. This was due to the reduced binding of TRF2-mediated REST/co-REST and LSD1 repressor complex (Mukherjee et al., 2018). In the case of the *hTERT* promoter, however, we observed significant change in the H3K27Me3 mark through TRF2-dependent engagement of the REST/PRC2 complex, whereas LSD1 occupancy remained unaffected (Figure S5G). The variation in the histone marks at the two promoters is likely due to the difference in the histone modifying complexes that TRF2 recruits at the two promoters. In addition, consistent with this, promoter-specific histone alterations on TRF2 silencing was found in multiple promoters studied by us earlier (Mukherjee et al., 2018, 2019a).

Further, the *hTERT* promoter was shown to coexist in multiple transient folded/unfolded states (Yu et al., 2012). This is consistent with our results suggesting that, in the presence of stabilizing ligands, the folded G-quadruplex form is promoted. This folded state is likely to result in enhanced TRF2 binding and/or disrupt the GABPA binding sites. In addition, because of reports showing *hTERT* G-quadruplex stabilization mask Sp1 and CTCF binding to the *hTERT* promoter (Li et al., 2017; Palumbo et al., 2009), the possibility of G-quadruplex-dependent mechanisms have been discussed (Kim et al., 2016; Li and Tergaonkar, 2016; Rhodes and Lipps, 2015). However, the role of *hTERT* promoter G-quadruplex-TRF2 interaction in directly determining the fate of telomerase regulation has not been reported earlier.

Consistent with our earlier results in case of *p21* and *PCGF3* promoters (Hussain et al., 2017; Purohit et al., 2018), we observed that both the N-terminal (B) and C-terminal (M) domains of TRF2 are important for binding at the *hTERT* promoter. The M domain was reported to be necessary for double-strand DNA binding at the telomeres (van Steensel et al., 1998). The B domain of TRF2 was reported in binding DNA secondary structures—e.g., in t-loop stabilization, double-single strand DNA junctions (Benarroch-Popivker et al., 2016; Fouché et al., 2006; Schmutz et al., 2017), and the G-quadruplex (Hussain et al., 2017; Mukherjee et al., 2019a; Pedroso et al., 2009; Purohit et al., 2018). It is possible, therefore, that binding of TRF2 outside telomeres, and particularly at promoters with DNA secondary structures, involves both M and B domains of full-length TRF2.

Moreover, DNA binding by TRF2 was shown to involve the homodimeric form of TRF2 (Choi et al., 2011; Court et al., 2005; van Steensel et al., 1998). Therefore, because in both TRF2-delB and TRF2-delM, where the dimerization domain is intact, the mutants would dimerize with the endogenous full-length TRF2. These interactions are likely to sequester endogenous TRF2 resulting in loss of TRF2 binding at the *hTERT* promoter. Similar observations were made for the loss of endogenous TRF2 from telomeres in presence of the TRF2-delM mutant (van Steensel et al., 1998). These resports also support our observations that the mutant forms not only do not bind to the *hTERT* promoter (Figure S1F) but also inhibit binding of the full-length endogenous TRF2 to the *hTERT* promoter (Figure S1H).

With the growing understanding of the function of telomerase in telomere protection in addition to telomere synthesis (Cesare et al., 2013; Perera et al., 2019; Sarthy and Baumann, 2010), mechanisms of telomerase regulation shown here, implicating potential crosstalk with telomeres, might be significant. Recently, we showed non-telomeric TRF2 binding to be telomere-dependent (Mukherjee et al., 2018, 2019a). Together, findings here might be relevant in further understanding how telomerase is regulated, and in turn how telomeres are managed/maintained during telomere-dependent physiological processes like cellular senescence, DNA damage response, cancer, and aging (Abbas and Dutta, 2009; Arnoult and Karlseder, 2015). The case of telomeres in cancer is particularly relevant. Although further work will be required to test this, based on our findings here, it is possible that establishment of a telomere-telomerase crosstalk through TRF2 (telomeric along with non-telomeric binding at the *hTERT* promoter) is key to how telomeres are managed in cancer cells. In addition, relatively enhanced levels of telomerase and long telomeres are crucial for maintenance/survival of pluripotent stem cells (Aguado et al., 2017; Vinayagamurthy et al., 2020; Zou et al., 2017) It is possible, therefore, that TRF2-mediated *hTERT* regulation, linked to telomeres, is of significance in pluripotency.

Kim et al. (2016) showed looping of the 5p chromosome telomere to a region ~1.2 Mb away and 100 kb downstream of *hTERT*. This loop further engaged the *hTERT* promoter, and as a consequence, authors concluded telomere-bound TRF2 was physically associated to the *hTERT* promoter. However, direct TRF2-dependent *hTERT* transcription was not studied. We show direct binding of TRF2 to the *hTERT* promoter that is independent of telomere looping. First, we reasoned telomere-association would show binding of other telomeric factors like TRF1, RAP1, and POT1 at the *hTERT* promoter along with TRF2—this was not the case (Figure 3E). Second, considering the likelihood of telomere looping to diminish with physical distance, we inserted an exogenous *hTERT* promoter-reporter ~46 Mb away from the nearest telomere. Here, again, TRF2 binding was clear whereas other telomere-bound factors were absent (Figures 3C and 3D). This is consistent with earlier work showing non-telomeric TRF2 binding throughout the genome (Mukherjee et al., 2018, 2019a). Therefore, it is likely that both telomere-dependent (Kim et al., 2016) and telomere-independent mechanisms of TRF2 interaction regulate *hTERT*. Further work will be required to understand in what contexts these mechanisms work, particularly with respect to aging (telomere shortening).

In conclusion, results showing TRF2-induced re-suppression of *hTERT* using small molecule ligands in GBM and other cancers offer potential therapeutic opportunity. We show mechanisms that maintain *hTERT* in a repressed state in normal cells. Deregulation of which induced *hTERT* reactivation in cancer cells. Together, these results suggest direct molecular links between telomeres and telomerase that might be critical in advancing the understanding of cell-intrinsic functions including neoplastic transformation, aging, and pluripotency/differentiation.

STAR★METHODS

Detailed methods are provided in the online version of this paper and include the following:

- KEY RESOURCES TABLE
- RESOURCE AVAILABILITY
  - Lead contact
  - Materials availability
  - Data and code availability
- EXPERIMENTAL MODEL AND SUBJECT DETAILS
  - Source and maintenance details of all **cancer, immortalized and primary** cell lines used in the study
  - Confirmation of the hTERT promoter mutations in patient-derived glioblastoma cells
  - CRISPR-mediated insertion of hTERT promoter-driven gaussia luciferase in to the CCR5 locus
  - Confirmation of CCR5-hTERT-Gaussia insert by sequencing and culture conditions
- METHODS DETAILS
  - Analysis of TERT promoter sequence across vertebrates for G-quadruplex
  - ChIP (chromatin immunoprecipitation)
  - Analysis of ChIP experiments-
  - Tel PCR
  - LSD1 chromatiniImmunoprecipitation
  - Re-ChIP
  - Immunoprecipitation of proteins
  - Immunofluorescence microscopy
  - Immuno-flow cytometry
  - Transfections and TRF2 silencing
  - GABPA silencing
  - TRF2 silencing recovery experiment
  - Gaussia-luciferase assay
  - Real time PCR for mRNA expression
  - Dot blot analysis
  - Western blotting
  - G-quadruplex preparation
  - Circular dichroism
  - ELISA
  - Telomerase activity using ELISA TRAP
  - Oligonucleotide-pulldown assay
  - TRF2 ChIP-seq coverage on TERT promoter
- QUANTIFICATION AND STATISTICAL ANALYSIS

SUPPLEMENTAL INFORMATION

Supplemental information can be found online at https://doi.org/10.1016/j.celrep.2021.109154.

ACKNOWLEDGMENTS

We thank Vinay Tergaonkar for the gift of cell lines with or without hTERT promoter mutations, Ellora Sen for GBM cell lines, and Lene Uhrbom and Smitha Sreedheran for U3013 GBM cells. We acknowledge Peter Mailliet for synthesis of G-quadruplex binding ligands used in this study. We are grateful to Balam Singh for laboratory management, Venkatesh Prasad for suggestions on immunofluorescence experiments, and Dr. Debayan Ganguly, Yasmeen Khan, and Dipanjali Sinha for helping with the CD experiments. We thank all members of the S.C. laboratory for their inputs/suggestions and the IGIB HPC and Core Imaging Facility. Research fellowships to S.S., A.K.M., S.S.R., A.S., M.K. (CSIR), S.B. (DBT), and M.V. (DST) are acknowledged. S.L. acknowledges Helse Sør-Øst, Norway and the Medical Student Research Program, University of Oslo, Oslo, Norway for fellowships. This work was supported by research grants from Wellcome Trust/DBT India Alliance Fellowship (IA/S/18/2/504021) to S.C. Support from Council of Scientific and Industrial Research (CSIR) and Department of Biotechnology (DBT) to S.C. and from Helse Sør-Øst, Norway and Medical Student Research Program, University of Oslo, Oslo, Norway to D.P. is also acknowledged.

AUTHOR CONTRIBUTIONS

S.S. did the TRF2 ChIP experiments and *hTERT* expression-related experiments, *hTERT* promoter activity assays, telomerase activity assays, immunofluorescence microscopy, ligand treatment experiments and downstream assays, histone ChIP, BG4 ChIP, oligonucleotide pull-down assays, ELISA, western blots for TRF2 silencing, and immunoprecipitation for REST and EZH2, ChIP for REST and EZH2, Re-CHIP for REST, FLAG ChIP for delB delM, TRF2 ChIP with DelB DelM overexpression, GABPA silencing experiments, GABPA ChIP followed by ligand overexpression, CD with ligand and CD with TRF2, data curation, *TERT* sequence homology across species, figures, and manuscript writing. A.K.M. did the histone ChIP assays, flow-cytometry, ChIP for shelterin components (TRF2, TRF1, RAP1, POT1), dot blots, ChIP and Re-CHIP for REST, *TERT* expression analysis, EZH2 ChIP, FLAG ChIP for delB delM, REST ChIP with DelB DelM overexpression, ChIP-seq reanalysis, data curation, figures, and manuscript writing. S.S.R. did the generation of *CCR5-TERT Gaussia* cell lines and characterization. S.B. did the TRF2 protein purification and TRF2 ChIP assays. S.L. and G.N. did the TRF2 ChIP and telomerase activity in patient-derived cell lines. D.P. did the TRF2 ChIP in patient-derived cell lines and telomerase activity and provided suggestions in manuscript. M.V. did the circular dichroism experiments. A.S. did the TRF2 protein purification. M.K. did the image acquisition for immunofluorescence experiments. S.C provided the conceptualization of the idea, design/plan of experiments, supervision, grants for funding, figures, and manuscript writing.

DECLARATION OF INTERESTS

S.C. is a scientific advisor for Rejuvas Biotech India Pvt. Ltd.

INCLUSION AND DIVERSITY

The author list of this paper includes contributors from the location where the research was conducted who participated in the data collection, design, analysis, and/or interpretation of the work.

Received: August 27, 2020
Revised: February 15, 2021
Accepted: April 28, 2021
Published: May 18, 2021

REFERENCES

Abbas, T., and Dutta, A. (2009). p21 in cancer: intricate networks and multiple activities. Nat. Rev. Cancer *9*, 400–414.

Aguado, T., Gutiérrez, F.J., Aix, E., Schneider, R.P., Giovinazzo, G., Blasco, M.A., and Flores, I. (2017). Telomere Length Defines the Cardiomyocyte

Differentiation Potency of Mouse Induced Pluripotent Stem Cells. Stem Cells *35*, 362–373.

Akıncılar, S.C., Khattar, E., Boon, P.L.S., Unal, B., Fullwood, M.J., and Tergaonkar, V. (2016). Long-Range Chromatin Interactions Drive Mutant TERT Promoter Activation. Cancer Discov. *6*, 1276–1291.

Arnoult, N., and Karlseder, J. (2015). Complex interactions between the DNA-damage response and mammalian telomeres. Nat. Struct. Mol. Biol. *22*, 859–866.

Artandi, S.E., and DePinho, R.A. (2010). Telomeres and telomerase in cancer. Carcinogenesis *31*, 9–18.

Bae, N.S., and Baumann, P. (2007). A RAP1/TRF2 complex inhibits nonhomologous end-joining at human telomeric DNA ends. Mol. Cell *26*, 323–334.

Baker, A.M., Fu, Q., Hayward, W., Lindsay, S.M., and Fletcher, T.M. (2009). The Myb/SANT domain of the telomere-binding protein TRF2 alters chromatin structure. Nucleic Acids Res. *37*, 5019–5031.

Balasubramanian, S., Hurley, L.H., and Neidle, S. (2011). Targeting G-quadruplexes in gene promoters: a novel anticancer strategy? Nat. Rev. Drug Discov. *10*, 261–275.

Baumann, P., and Price, C. (2010). Pot1 and telomere maintenance. FEBS Lett. *584*, 3779–3784.

Bell, R.J.A., Rube, H.T., Kreig, A., Mancini, A., Fouse, S.D., Nagarajan, R.P., Choi, S., Hong, C., He, D., Pekmezci, M., et al. (2015). Cancer. The transcription factor GABP selectively binds and activates the mutant TERT promoter in cancer. Science *348*, 1036–1039.

Benarroch-Popivker, D., Pisano, S., Mendez-Bermudez, A., Lototska, L., Kaur, P., Bauwens, S., Djerbi, N., Latrick, C.M., Fraisier, V., Pei, B., et al. (2016). TRF2-Mediated Control of Telomere DNA Topology as a Mechanism for Chromosome-End Protection. Mol. Cell *61*, 274–286.

Benetti, R., Schoeftner, S., Muñoz, P., and Blasco, M.A. (2008). Role of TRF2 in the assembly of telomeric chromatin. Cell Cycle *7*, 3461–3468.

Biffi, G., Tannahill, D., and Balasubramanian, S. (2012). An intramolecular G-quadruplex structure is required for binding of telomeric repeat-containing RNA to the telomeric protein TRF2. J. Am. Chem. Soc. *134*, 11974–11976.

Blackburn, E.H., Greider, C.W., and Szostak, J.W. (2006). Telomeres and telomerase: the path from maize, Tetrahymena and yeast to human cancer and aging. Nat. Med. *12*, 1133–1138.

Brien, G.L., Valerio, D.G., and Armstrong, S.A. (2016). Exploiting the Epigenome to Control Cancer-Promoting Gene-Expression Programs. Cancer Cell *29*, 464–476.

Broccoli, D., Young, J.W., and de Lange, T. (1995). Telomerase activity in normal and malignant hematopoietic cells. Proc. Natl. Acad. Sci. USA *92*, 9082–9086.

Bruce, A.W., Donaldson, I.J., Wood, I.C., Yerbury, S.A., Sadowski, M.I., Chapman, M., Göttgens, B., and Buckley, N.J. (2004). Genome-wide analysis of repressor element 1 silencing transcription factor/neuron-restrictive silencing factor (REST/NRSF) target genes. Proc. Natl. Acad. Sci. USA *101*, 10458–10463.

Bryan, T.M., and Baumann, P. (2011). G-quadruplexes: from guanine gels to chemotherapeutics. Mol. Biotechnol. *49*, 198–208.

Calvete, O., Martinez, P., Garcia-Pavia, P., Benitez-Buelga, C., Paumard-Hernández, B., Fernandez, V., Dominguez, F., Salas, C., Romero-Laorden, N., Garcia-Donas, J., et al. (2015). A mutation in the POT1 gene is responsible for cardiac angiosarcoma in TP53-negative Li-Fraumeni-like families. Nat. Commun. *6*, 8383.

Cao, Y., Li, H., Deb, S., and Liu, J.-P. (2002). TERT regulates cell survival independent of telomerase enzymatic activity. Oncogene *21*, 3130–3138.

Cech, T.R. (2004). Beginning to understand the end of the chromosome. Cell *116*, 273–279.

Cesare, A.J., Hayashi, M.T., Crabbe, L., and Karlseder, J. (2013). The telomere deprotection response is functionally distinct from the genomic DNA damage response. Mol. Cell *51*, 141–155.

Choi, K.H., Farrell, A.S., Lakamp, A.S., and Ouellette, M.M. (2011). Characterization of the DNA binding specificity of Shelterin complexes. Nucleic Acids Res. *39*, 9206–9223.

Chow, T.T., Shi, X., Wei, J.-H., Guan, J., Stadler, G., Huang, B., and Blackburn, E.H. (2018). Local enrichment of HP1alpha at telomeres alters their structure and regulation of telomere protection. Nat. Commun. *9*, 3583.

Collie, G.W., Promontorio, R., Hampel, S.M., Micco, M., Neidle, S., and Parkinson, G.N. (2012). Structural basis for telomeric G-quadruplex targeting by naphthalene diimide ligands. J. Am. Chem. Soc. *134*, 2723–2731.

Cong, Y.-S., Wright, W.E., and Shay, J.W. (2002). Human telomerase and its regulation. Microbiol. Mol. Biol. Rev. *66*, 407–425.

Court, R., Chapman, L., Fairall, L., and Rhodes, D. (2005). How the human telomeric proteins TRF1 and TRF2 recognize telomeric DNA: a view from high-resolution crystal structures. EMBO Rep. *6*, 39–45.

Cristofari, G., and Lingner, J. (2006). Telomere length homeostasis requires that telomerase levels are limiting. EMBO J. *25*, 565–574.

Dash, J., Shirude, P.S., and Balasubramanian, S. (2008). G-quadruplex recognition by bis-indole carboxamides. Chem. Commun. (Camb.) (*26*), 3055–3057.

Dhapola, P., and Chowdhury, S. (2016). QuadBase2: web server for multiplexed guanine quadruplex mining and visualization. Nucleic Acids Res. *44* (*W1*), W277-83.

Dietrich, N., Lerdrup, M., Landt, E., Agrawal-Singh, S., Bak, M., Tommerup, N., Rappsilber, J., Södersten, E., and Hansen, K. (2012). REST-mediated recruitment of polycomb repressor complexes in mammalian cells. PLoS Genet. *8*, e1002494.

Edgar, R.C. (2004). MUSCLE: multiple sequence alignment with high accuracy and high throughput. Nucleic Acids Res. *32*, 1792–1797.

El Maï, M., Wagner, K.-D., Michiels, J.-F., Ambrosetti, D., Borderie, A., Destree, S., Renault, V., Djerbi, N., Giraud-Panis, M.-J., Gilson, E., and Wagner, N. (2014). The Telomeric Protein TRF2 Regulates Angiogenesis by Binding and Activating the PDGFRβ Promoter. Cell Rep. *9*, 1047–1060.

Escoffier, E., Rezza, A., Roborel de Climens, A., Belleville, A., Gazzolo, L., Gilson, E., and Duc Dodon, M. (2005). A balanced transcription between telomerase and the telomeric DNA-binding proteins TRF1, TRF2 and Pot1 in resting, activated, HTLV-1-transformed and Tax-expressing human T lymphocytes. Retrovirology *2*, 77.

Fael Al-Mayhani, T.M., Ball, S.L.R., Zhao, J.-W., Fawcett, J., Ichimura, K., Collins, P.V., and Watts, C. (2009). An efficient method for derivation and propagation of glioblastoma cell lines that conserves the molecular profile of their original tumours. J. Neurosci. Methods *176*, 192–199.

Fouché, N., Cesare, A.J., Willcox, S., Ozgür, S., Compton, S.A., and Griffith, J.D. (2006). The basic domain of TRF2 directs binding to DNA junctions irrespective of the presence of TTAGGG repeats. J. Biol. Chem. *281*, 37486–37495.

Giri, S., Nieber, K., Acikgöz, A., Pavlica, S., Keller, M., and Bader, A. (2010). Telomerase activity and hepatic functions of rat embryonic liver progenitor cell in nanoscaffold-coated model bioreactor. In Molecular and Cellular Biochemistry (Springer), pp. 137–149.

Granotier, C., Pennarun, G., Riou, L., Hoffschir, F., Gauthier, L.R., De Cian, A., Gomez, D., Mandine, E., Riou, J.F., Mergny, J.L., et al. (2005). Preferential binding of a G-quadruplex ligand to human chromosome ends. Nucleic Acids Res. *33*, 4182–4190.

Hampel, S.M., Sidibe, A., Gunaratnam, M., Riou, J.F., and Neidle, S. (2010). Tetrasubstituted naphthalene diimide ligands with selectivity for telomeric G-quadruplexes and cancer cells. Bioorg. Med. Chem. Lett. *20*, 6459–6463.

Hänsel-Hertsch, R., Spiegel, J., Marsico, G., Tannahill, D., and Balasubramanian, S. (2018). Genome-wide mapping of endogenous G-quadruplex DNA structures by chromatin immunoprecipitation and high-throughput sequencing. Nat. Protoc. *13*, 551–564.

Horn, S., Figl, A., Rachakonda, P.S., Fischer, C., Sucker, A., Gast, A., Kadel, S., Moll, I., Nagore, E., Hemminki, K., et al. (2013). TERT promoter mutations in familial and sporadic melanoma. Science *339*, 959–961.

Huang, F.W., Hodis, E., Xu, M.J., Kryukov, G.V., Chin, L., and Garraway, L.A. (2013). Highly recurrent TERT promoter mutations in human melanoma. Science *339*, 957–959.

Hussain, T., Saha, D., Purohit, G., Kar, A., Kishore Mukherjee, A., Sharma, S., Sengupta, S., Dhapola, P., Maji, B., Vedagopuram, S., et al. (2017). Transcription regulation of CDKN1A (p21/CIP1/WAF1) by TRF2 is epigenetically controlled through the REST repressor complex. Sci. Rep. *7*, 11541.

Islam, M.A., Thomas, S.D., Murty, V.V., Sedoris, K.J., and Miller, D.M. (2014). c-Myc quadruplex-forming sequence Pu-27 induces extensive damage in both telomeric and nontelomeric regions of DNA. J. Biol. Chem. *289*, 8521–8531.

Janoušková, E., Nečasová, I., Pavloušková, J., Zimmermann, M., Hluchý, M., Marini, V., Nováková, M., and Hofr, C. (2015). Human Rap1 modulates TRF2 attraction to telomeric DNA. Nucleic Acids Res. *43*, 2691–2700.

Kang, H.-J., Cui, Y., Yin, H., Scheid, A., Hendricks, W.P.D., Schmidt, J., Sekulic, A., Kong, D., Trent, J.M., Gokhale, V., et al. (2016). A Pharmacological Chaperone Molecule Induces Cancer Cell Death by Restoring Tertiary DNA Structures in Mutant hTERT Promoters. J. Am. Chem. Soc. *138*, 13673–13692.

Killedar, A., Stutz, M.D., Sobinoff, A.P., Tomlinson, C.G., Bryan, T.M., Beesley, J., Chenevix-Trench, G., Reddel, R.R., and Pickett, H.A. (2015). A Common Cancer Risk-Associated Allele in the hTERT Locus Encodes a Dominant Negative Inhibitor of Telomerase. PLoS Genet. *11*, e1005286.

Killela, P.J., Reitman, Z.J., Jiao, Y., Bettegowda, C., Agrawal, N., Diaz, L.A., Jr., Friedman, A.H., Friedman, H., Gallia, G.L., Giovanella, B.C., et al. (2013). TERT promoter mutations occur frequently in gliomas and a subset of tumors derived from cells with low rates of self-renewal. Proc. Natl. Acad. Sci. USA *110*, 6021–6026.

Kim, N.W., Piatyszek, M.A., Prowse, K.R., Harley, C.B., West, M.D., Ho, P.L., Coviello, G.M., Wright, W.E., Weinrich, S.L., and Shay, J.W. (1994). Specific association of human telomerase activity with immortal cells and cancer. Science *266*, 2011–2015.

Kim, W., Ludlow, A.T., Min, J., Robin, J.D., Stadler, G., Mender, I., Lai, T.-P., Zhang, N., Wright, W.E., and Shay, J.W. (2016). Regulation of the Human Telomerase Gene TERT by Telomere Position Effect-Over Long Distances (TPE-OLD): Implications for Aging and Cancer. PLoS Biol. *14*, e2000016.

Kyo, S., Takakura, M., Kohama, T., and Inoue, M. (1997). Telomerase activity in human endometrium. Cancer Res. *57*, 610–614.

Li, Y., and Tergaonkar, V. (2016). Telomerase reactivation in cancers: Mechanisms that govern transcriptional activation of the wild-type vs. mutant TERT promoters. Transcription *7*, 44–49.

Li, Y., Zhou, Q.-L., Sun, W., Chandrasekharan, P., Cheng, H.S., Ying, Z., Lakshmanan, M., Raju, A., Tenen, D.G., Cheng, S.-Y., et al. (2015). Non-canonical NF-κB signalling and ETS1/2 cooperatively drive C250T mutant TERT promoter activation. Nat. Cell Biol. *17*, 1327–1338.

Li, P.-T., Wang, Z.-F., Chu, I.-T., Kuan, Y.-M., Li, M.-H., Huang, M.-C., Chiang, P.-C., Chang, T.-C., and Chen, C.-T. (2017). Expression of the human telomerase reverse transcriptase gene is modulated by quadruplex formation in its first exon due to DNA methylation. J. Biol. Chem. *292*, 20859–20870.

Lim, K.W., Lacroix, L., Yue, D.J.E., Lim, J.K.C., Lim, J.M.W., and Phan, A.T. (2010). Coexistence of two distinct G-quadruplex conformations in the hTERT promoter. J. Am. Chem. Soc. *132*, 12331–12342.

Liu, T., Yuan, X., and Xu, D. (2016). Cancer-Specific Telomerase Reverse Transcriptase (TERT) Promoter Mutations: Biological and Clinical Implications. Genes (Basel) *7*, 38.

Margueron, R., and Reinberg, D. (2011). The Polycomb complex PRC2 and its mark in life. Nature *469*, 343–349.

Martinez, P., Thanasoula, M., Carlos, A.R., Gómez-López, G., Tejera, A.M., Schoeftner, S., Dominguez, O., Pisano, D.G., Tarsounas, M., and Blasco, M.A. (2010). Mammalian Rap1 controls telomere function and gene expression through binding to telomeric and extratelomeric sites. Nat. Cell Biol. *12*, 768–780.

Masutomi, K., Yu, E.Y., Khurts, S., Ben-Porath, I., Currier, J.L., Metz, G.B., Brooks, M.W., Kaneko, S., Murakami, S., DeCaprio, J.A., et al. (2003). Telomerase maintains telomere structure in normal human cells. Cell *114*, 241–253.

McGann, J.C., Oyer, J.A., Garg, S., Yao, H., Liu, J., Feng, X., Liao, L., Yates, J.R., 3rd, and Mandel, G. (2014). Polycomb- and REST-associated histone deacetylases are independent pathways toward a mature neuronal phenotype. eLife *3*, e04235.

Mergny, J.-L., Riou, J.F., Mailliet, P., Teulade-Fichou, M.P., and Gilson, E. (2002). Natural and pharmacological regulation of telomerase. Nucleic Acids Res. *30*, 839–865.

Mishra, S.K., Tawani, A., Mishra, A., and Kumar, A. (2016). G4IPDB: A database for G-quadruplex structure forming nucleic acid interacting proteins. Sci. Rep. *6*, 38144.

Monsen, R.C., DeLeeuw, L., Dean, W.L., Gray, R.D., Sabo, T.M., Chakravarthy, S., Chaires, J.B., and Trent, J.O. (2020). The hTERT core promoter forms three parallel G-quadruplexes. Nucleic Acids Res. *48*, 5720–5734.

Mukherjee, A.K., Sharma, S., Sengupta, S., Saha, D., Kumar, P., Hussain, T., Srivastava, V., Roy, S.D., Shay, J.W., and Chowdhury, S. (2018). Telomere length-dependent transcription and epigenetic modifications in promoters remote from telomere ends. PLoS Genet. *14*, e1007782.

Mukherjee, A.K., Sharma, S., Bagri, S., Kutum, R., Kumar, P., Hussain, A., Singh, P., Saha, D., Kar, A., Dash, D., and Chowdhury, S. (2019a). Telomere repeat-binding factor 2 binds extensively to extra-telomeric G-quadruplexes and regulates the epigenetic status of several gene promoters. J. Biol. Chem. *294*, 17709–17722.

Mukherjee, A.K., Sharma, S., and Chowdhury, S. (2019b). Non-duplex G-Quadruplex Structures Emerge as Mediators of Epigenetic Modifications. Trends Genet. *35*, 129–144.

O'Callaghan, N., Dhillon, V., Thomas, P., and Fenech, M. (2008). A quantitative real-time PCR method for absolute telomere length. Biotechniques *44*, 807–809.

Paeschke, K., Simonsson, T., Postberg, J., Rhodes, D., and Lipps, H.J. (2005). Telomere end-binding proteins control the formation of G-quadruplex DNA structures in vivo. Nat. Struct. Mol. Biol. *12*, 847–854.

Palumbo, S.L., Ebbinghaus, S.W., and Hurley, L.H. (2009). Formation of a unique end-to-end stacked pair of G-quadruplexes in the hTERT core promoter with implications for inhibition of telomerase by G-quadruplex-interactive ligands. J. Am. Chem. Soc. *131*, 10878–10891.

Pandita, R.K., Chow, T.T., Udayakumar, D., Bain, A.L., Cubeddu, L., Hunt, C.R., Shi, W., Horikoshi, N., Zhao, Y., Wright, W.E., et al. (2015). Single-strand DNA-binding protein SSB1 facilitates TERT recruitment to telomeres and maintains telomere G-overhangs. Cancer Res. *75*, 858–869.

Patil, V., Pal, J., and Somasundaram, K. (2015). Elucidating the cancer-specific genetic alteration spectrum of glioblastoma derived cell lines from whole exome and RNA sequencing. Oncotarget *6*, 43452–43471.

Pedroso, I.M., Hayward, W., and Fletcher, T.M. (2009). The effect of the TRF2 N-terminal and TRFH regions on telomeric G-quadruplex structures. Nucleic Acids Res. *37*, 1541–1554.

Perera, O.N., Sobinoff, A.P., Teber, E.T., Harman, A., Maritz, M.F., Yang, S.F., Pickett, H.A., Cesare, A.J., Arthur, J.W., MacKenzie, K.L., and Bryan, T.M. (2019). Telomerase promotes formation of a telomere protective complex in cancer cells. Sci. Adv. *5*, eaav4409.

Pike, A.M., Strong, M.A., Ouyang, J.P.T., and Greider, C.W. (2019). TIN2 Functions with TPP1/POT1 To Stimulate Telomerase Processivity. Mol. Cell. Biol. *39*, e00593-18.

Pollard, S.M., Yoshikawa, K., Clarke, I.D., Danovi, D., Stricker, S., Russell, R., Bayani, J., Head, R., Lee, M., Bernstein, M., et al. (2009). Glioma stem cell lines expanded in adherent culture have tumor-specific phenotypes and are suitable for chemical and genetic screens. Cell Stem Cell *4*, 568–580.

Purohit, G., Mukherjee, A.K., Sharma, S., and Chowdhury, S. (2018). Extratelomeric Binding of the Telomere Binding Protein TRF2 at the PCGF3 Promoter Is G-Quadruplex Motif-Dependent. Biochemistry *57*, 2317–2324.

Rhodes, D., and Lipps, H.J. (2015). G-quadruplexes and their regulatory roles in biology. Nucleic Acids Res. *43*, 8627–8637.

Roach, R.J., Garavís, M., González, C., Jameson, G.B., Filichev, V.V., and Hale, T.K. (2020). Heterochromatin protein 1α interacts with parallel RNA and DNA G-quadruplexes. Nucleic Acids Res. *48*, 682–693.

Saha, D., Singh, A., Hussain, T., Srivastava, V., Sengupta, S., Kar, A., Dhapola, P., Dhople, V., Ummanni, R., and Chowdhury, S. (2017). Epigenetic suppression of human telomerase (*hTERT*) is mediated by the metastasis suppressor NME2 in a G-quadruplex-dependent fashion. J. Biol. Chem. *292*, 15205–15215.

Sarthy, J.F., and Baumann, P. (2010). Apollo-taking the lead in telomere protection. Mol. Cell *39*, 489–491.

Sarthy, J., Bae, N.S., Scrafford, J., and Baumann, P. (2009). Human RAP1 inhibits non-homologous end joining at telomeres. EMBO J. *28*, 3390–3399.

Savary, K., Caglayan, D., Caja, L., Tzavlaki, K., Bin Nayeem, S., Bergström, T., Jiang, Y., Uhrbom, L., Forsberg-Nilsson, K., Westermark, B., et al. (2013). Snail depletes the tumorigenic potential of glioblastoma. Oncogene *32*, 5409–5420.

Schmutz, I., Timashev, L., Xie, W., Patel, D.J., and de Lange, T. (2017). TRF2 binds branched DNA to safeguard telomere integrity. Nat. Struct. Mol. Biol. *24*, 734–742.

Shay, J.W., and Bacchetti, S. (1997). A survey of telomerase activity in human cancer. Eur. J. Cancer *33*, 787–791.

Shay, J.W., and Wright, W.E. (2019). Telomeres and telomerase: three decades of progress. Nat. Rev. Genet. *20*, 299–309.

Shi, Y.-A., Zhao, Q., Zhang, L.-H., Du, W., Wang, X.-Y., He, X., Wu, S., and Li, Y.-L. (2014). Knockdown of hTERT by siRNA inhibits cervical cancer cell growth in vitro and in vivo. Int. J. Oncol. *45*, 1216–1224.

Simonet, T., Zaragosi, L.-E., Philippe, C., Lebrigand, K., Schouteden, C., Augereau, A., Bauwens, S., Ye, J., Santagostino, M., Giulotto, E., et al. (2011). The human TTAGGG repeat factors 1 and 2 bind to a subset of interstitial telomeric sequences and satellite repeats. Cell Res. *21*, 1028–1038.

Smekalova, E., and Baumann, P. (2013). TERRA -a calling card for telomerase. Mol. Cell *51*, 703–704.

Smogorzewska, A., van Steensel, B., Bianchi, A., Oelmann, S., Schaefer, M.R., Schnapp, G., and de Lange, T. (2000). Control of human telomere length by TRF1 and TRF2. Mol. Cell. Biol. *20*, 1659–1668.

Stern, J.L., Theodorescu, D., Vogelstein, B., Papadopoulos, N., and Cech, T.R. (2015). Mutation of the TERT promoter, switch to active chromatin, and monoallelic TERT expression in multiple cancers. Genes Dev. *29*, 2219–2224.

Stern, J.L., Paucek, R.D., Huang, F.W., Ghandi, M., Nwumeh, R., Costello, J.C., and Cech, T.R. (2017). Allele-Specific DNA Methylation and Its Interplay with Repressive Histone Marks at Promoter-Mutant TERT Genes. Cell Rep. *21*, 3700–3707.

Tomlinson, C.G., Moye, A.L., Holien, J.K., Parker, M.W., Cohen, S.B., and Bryan, T.M. (2015). Two-step mechanism involving active-site conformational changes regulates human telomerase DNA binding. Biochem. J. *465*, 347–357.

Traczyk, A., Liew, C.W., Gill, D.J., and Rhodes, D. (2020). Structural basis of G-quadruplex DNA recognition by the yeast telomeric protein Rap1. Nucleic Acids Res. *48*, 4562–4571.

Valentijn, L.J., Koster, J., Zwijnenburg, D.A., Hasselt, N.E., van Sluis, P., Volckmann, R., van Noesel, M.M., George, R.E., Tytgat, G.A.M., Molenaar, J.J., and Versteeg, R. (2015). TERT rearrangements are frequent in neuroblastoma and identify aggressive tumors. Nat. Genet. *47*, 1411–1414.

van Steensel, B., Smogorzewska, A., and de Lange, T. (1998). TRF2 protects human telomeres from end-to-end fusions. Cell *92*, 401–413.

Vinayagamurthy, S., Ganguly, A., and Chowdhury, S. (2020). Extra-telomeric impact of telomeres: Emerging molecular connections in pluripotency or stemness. J. Biol. Chem. *295*, 10245–10254.

Wong, M.S., Wright, W.E., and Shay, J.W. (2014). Alternative splicing regulation of telomerase: a new paradigm? Trends Genet. *30*, 430–438.

Xie, Y., Bergström, T., Jiang, Y., Johansson, P., Marinescu, V.D., Lindberg, N., Segerman, A., Wicher, G., Niklasson, M., Baskaran, S., et al. (2015). The Human Glioblastoma Cell Culture Resource: Validated Cell Models Representing All Molecular Subtypes. EBioMedicine *2*, 1351–1363.

Yang, D., Xiong, Y., Kim, H., He, Q., Li, Y., Chen, R., and Songyang, Z. (2011). Human telomeric proteins occupy selective interstitial sites. Cell Res. *21*, 1013–1027.

Ye, J., Renault, V.M., Jamet, K., and Gilson, E. (2014). Transcriptional outcome of telomere signalling. Nat. Rev. Genet. *15*, 491–503.

Yu, Z., Gaerig, V., Cui, Y., Kang, H., Gokhale, V., Zhao, Y., Hurley, L.H., and Mao, H. (2012). Tertiary DNA structure in the single-stranded hTERT promoter fragment unfolds and refolds by parallel pathways via cooperative or sequential events. J. Am. Chem. Soc. *134*, 5157–5164.

Zaug, A.J., Podell, E.R., and Cech, T.R. (2005). Human POT1 disrupts telomeric G-quadruplexes allowing telomerase extension in vitro. Proc. Natl. Acad. Sci. USA *102*, 10864–10869.

Zhang, P., Casaday-Potts, R., Precht, P., Jiang, H., Liu, Y., Pazin, M.J., and Mattson, M.P. (2011). Nontelomeric splice variant of telomere repeat-binding factor 2 maintains neuronal traits by sequestering repressor element 1-silencing transcription factor. Proc. Natl. Acad. Sci. USA *108*, 16434–16439.

Zou, Y., Tong, H.J., Li, M., Tan, K.S., and Cao, T. (2017). Telomere length is regulated by FGF-2 in human embryonic stem cells and affects the life span of its differentiated progenies. Biogerontology *18*, 69–84.

STAR★METHODS

KEY RESOURCES TABLE

REAGENT or RESOURCE	SOURCE	IDENTIFIER
Antibodies		
TRF2 rabbit polyclonal	Novus	Cat#NB110-57130; RRID:AB_844199
TRF2 mouse monoclonal	Abcam	Cat#4A794 ab13579; RRID:AB_300474
hTERT rabbit monoclonal Y182	Abcam	Cat#ab32020; RRID:AB_778296
REST rabbit polyclonal	Millipore	Cat#17-641; RRID:AB_11212617
Histone H3 rabbit polyclonal	Abcam	Cat# ab1791; RRID:AB_302613
H3K4me1 rabbit polyclonal	Abcam	Cat# ab8895; RRID:AB_306847
H3K4me3 mouse monoclonal	Abcam	Cat# ab1012; RRID:AB_442796
H3K27me3 mouse monoclonal	Abcam	Cat# ab6002; RRID:AB_305237
H3K9me3 rabbit polyclonal	Abcam	Cat# ab176916; RRID:AB_2797591
BG4 G4 specific antibody monoclonal	Millipore	Cat# MABE917; RRID:AB_2750936
EZH2 rabbit polyclonal	Cell Signaling Technologies	Cat#4905; RRID:AB_2278249
GAPDH mouse monoclonal	Santacruz	Cat#6C5 SC-32233; RRID:AB_627679
TRF1 mouse monoclonal	Novus	Cat# NB110-68281; RRID:AB_1111093
RAP1 mouse monoclonal	Santa Cruz	Cat#4C8/1 SC-53434; RRID:AB_630189
POT1 mouse monoclonal	Santacruz	Cat# M1P1H5 SC-81711; RRID:AB_1128696
Monoclonal anti-FLAG M2 Mouse antibody	Sigma	Cat# F1804; RRID:AB_262044
LSD1 primary anti-rabbit antibody	Cell Signaling Technologies	Cat#2139; RRID:AB_2070135
anti-Rabbit-HRP	Cell Signaling Technologies	Cat#7074S; RRID:AB_2099233
anti-Mouse-HRP	Cell Signaling Technologies	Cat#7076S; RRID:AB_330924
anti-rabbit Alexa Fluor® 488	Molecular Probes, Life Technologies	Cat#A11034; RRID:AB_2576217
anti-mouse Alexa Fluor® 594	Molecular Probes, Life Technologies	Cat#A11062; RRID:AB_1500656
Critical commercial assays		
Qubit dsDNA HS Assay Kit	Invitrogen	Cat#Q32851
Magnetic Dyna- beads (protein G/A) for immunoprecipitation	Invitrogen	Cat# 10009D
FUGENE HD	Promega	Cat# E2311
Amersham Rapid-Hyb buffer	GE healthcare	Cat#RPN1635
TeloTAGGG Telomerase PCR ELISA kit	Sigma Millipore Merck	Cat#11854666910
Experimental models: Cell lines		
HT1080	ATCC	Cat#ATCC-CCL-121
MRC5	ATCC	Cat#ATCC® CCL-171
HEK293T	ATCC	Cat#ATCC® CRL-3216
HCT116	Gift form Prof.Vinay Tergaonkar laboratory	N/A
U87MG	Gift from Prof. Ellora Sen laboratory	N/A
LN229	Gift from Prof. Ellora Sen laboratory	N/A
Oligonucleotides		
hTERT (+38 to −237) FP- CCAGGCCGGGCTCCCAGTGGAT	This paper	N/A
hTERT (+38 to −237) RP- GGCTTCCCACGTGCGCAGCAGGA	This paper	N/A
ChIP-q-PCR Primers used for hTERT-gaussia inserted at the CCR5 locus FP GACCGCGCTTCCCACGTGGCGGAG	This paper	N/A

(*Continued on next page*)

Continued

REAGENT or RESOURCE	SOURCE	IDENTIFIER
ChIP-q-PCR Primers used for hTERT-gaussia inserted at the CCR5 locus RP GCCTCGGCCACAGCGATGCAGATCAG	This paper	N/A
Tel PCRFP-CGGTTTGTTTGGGTTTG GGTTTGGGTTTGGGTTTGGGTT	This paper	N/A
Tel PCRRP- GGCTTGCCTTACCCT TACCCTTACCCTTACCCTTACCCT	This paper	N/A
gRNA sequence GGAGAGCTTGGCTCTGTTGGGGG	This paper	Sigma (custom synthesis)
TRF2 siRNA 5′GGCUGGAGUGCAGAAAUAU3′	This paper	N/A
TRF2 siRNA 5′CUGGGCUGCCAUUUCUAAA3′	This paper	N/A
TRF2 siRNA 5′GCUGCUGUCAUUAUUUGUA3′	This paper	N/A
For other oligonucleotides, refer to supplemental information	N/A	N/A
Recombinant DNA		
AY10_pS. Donor.R5.TS	Addgene	Cat#100292
hTERT promoter driven Gaussia Luciferase insert construct	Genecopoeia	Cat# HPRM25711-PG04
pX459 v2.0	Gift from Feng Zhang lab	N/A
TRF2 overexpression pCMV6 plasmid	Origene	Cat#PS100001
AY10_pS. Donor.R5.TS	Addgene	Cat#100292
Software and algorithms		
Quadbase 2 server for G-quadruplex detection	Dhapola and Chowdhury, 2016	http://quadbase.igib.res.in/TetraPlexFinder
MUSCLE for sequence alignment	Edgar, 2004	https://www.ebi.ac.uk/Tools/msa/muscle/
Prism 8 Graphpad Prism	https://www.graphpad.com/scientific-software/prism/	N/A
G-quadruplex binding ligands		
260697	Mergny et al., 2002; gift from Jean Francois Riou's laboratory	N/A
FC4ND08	Collie et al., 2012; gift from Jean Francois Riou's laboratory	N/A
SMH1-4.6	Hampel et al., 2010; gift from Jean Francois Riou's laboratory	N/A
JD83	Dash et al., 2008; gift from Jean Francois Riou's laboratory	N/A

RESOURCE AVAILABILITY

Lead contact

Further information and requests for resources and reagents should be directed to and will be fulfilled by the lead contact, Shantanu Chowdhury (shantanuc@igib.in).

Materials availability

Reagents generated in this study are available from the lead contact with a completed materials transfer agreement.

Data and code availability

This study did not generate datasets/code.

EXPERIMENTAL MODEL AND SUBJECT DETAILS

Source and maintenance details of all cancer, immortalized and primary cell lines used in the study

Cancer cell lines

HT1080 fibrosarcoma cell line was purchased from ATCC (ATCC-CCL-121) and cultured in Modified Eagle's medium (MEM) supplemented with 10% Fetal Bovine Serum (FBS). HCT116 colorectal cancer cell line was a Gift from Prof. Vinay Tergaonkar's lab, these were cultured in Dulbecco's Modified Eagle's Medium-High Glucose (DMEM-HG) supplemented with 10% FBS with 1X Anti-Anti. U87MG and LN229 Glioblastoma cell lines were a kind gift from Prof. Ellora Sen from NBRC, these were both cultured in DMEM-HG with 1X Glutamax, 1X Anti-Anti (GIBCO) and 10% FBS. All cell lines were maintained at 37 Degree Celsius, with 5% CO_2 and 95% humidity.

hTERT promoter mutant isogenic cell lines

Isogneic pairs of HCT116, T98G and BLM cells with their respective *hTERT* promoter mutant cell lines were a kind gift form Prof. Vinay Tergaonkar's lab. These were all maintained in Dulbecco's Modified Eagle's Medium-High Glucose (DMEM-HG) supplemented with 10% FBS with 1X Anti-Anti. All cell lines were maintained at 37 Degree Celsius, with 5% CO_2 and 95% humidity.

Primary and Normal immortalized cell lines

MRC5 Primary fibroblasts were obtained from ATCC (ATCC® CCL-171) and cultured in Modified Eagle's medium (MEM) supplemented with 10% Fetal Bovine Serum (FBS) and 1x Glutamax with 1X Anti-Anti. HEK293T (human embryonic kidney normal immortalized cell line) was also obtained from ATCC (ATCC® CRL-3216) and cultured in Dulbecco's Modified Eagle's Medium-High Glucose (DMEM-HG) supplemented with 10% FBS. All cell lines were maintained at 37 Degree Celsius, with 5% CO_2 and 95% humidity.

Primary Glioblastoma cell lines

Primary glioma patient-derived cell lines G144 (51yr old male) and G166 (74yr old female) were as reported (Pollard et al., 2009). U3013 cell line (derived from 78yr old female) (Savary et al., 2013; Xie et al., 2015). G14 and G7 cells were first reported in Fael Al-Mayhani et al. (2009) and Pollard et al. (2009); however no patient information was available in the earlier reports or could be retrieved by us. G144, G166, G14 and G7 were kind gift from Dr. Steve Pollard, Edinburgh. These cells were cultured by Dr. Deo Prakash Pandey's laboratory as described in Pollard et al., 2009. U3013, was a gift from Prof. Lene Uhrnbom and these were cultured according to protocol stated in Savary et al. (2013) and Xie et al. (2015). All cell lines were maintained at 37°C, with 5% CO2 and 95% humidity.

Confirmation of the hTERT promoter mutations in patient-derived glioblastoma cells

Bases corresponding to −146 or −124 mutation are marked in green (wild-type) or red (in case of mutation) below.

G144

CCTCGCCGTTGGGAGCAATGCTGCCCGTGGGAGCCCAGGGGACCCGGGCACCCGTCCTGCCCCTTCACCTTCCAGCTCCG
CCTCCTCCGCGCGGACCCCGCCCCGTCCCGACCCCT**C**CCGGGTCCCCGGCCCAGCCCC**C**TCCGGGCCCTCCCAGCC
CCTCCCCTTCCTTTCCGCGGCCCCGCCCTCTCCTCGCGGCGCGAGTTTCAGGCAGCGCTGCGTCCTGCTGCGCACGTGG-
GAAGCCCCT

No mutations (WT)

G7

GAACTAATAGAGATGTAAGCGTGTTGAAGCGATGGCGGAGGGACTAGGGGACCCGGGCACCCGTCCTGCCCCTTCACCTTC-
CAGCTCCGCCTCCTCCGCGCGGACCCCGCCCCGTCCCGACCCCT**C**CCGGGTCCCCGGCCCAGCCCC**T**TCCGGGCCCTCC-
CAGCCCCTCCCCTTCCTTTCCGCGGCCCCGCCCTCTCCTCGCGGCGCGAGTTTCAGGCAGCGCTGCGTCCTGCTGCGCA
CGTGGGAAGCC

−124 C > T/G > A mutation

G166

GAACTAATAGAGATGTAAGCGTGTTGAAGCGATGGCGGAGGGACTAGGGGACCCGGGCACCCGTCCTGCCCCTTCACCTTC-
CAGCTCCGCCTCCTCCGCGCGGACCCCGCCCCGTCCCGACCCCT**C**CCGGGTCCCCGGCCCAGCCCC**T**TCCGGGCCCTCC-
CAGCCCCTCCCCTTCCTTTCCGCGGCCCCGCCCTCTCCTCGCGGCGCGAGTTTCAGGCAGCGCTGCGTCCTGCTGCGCAC
GTGGGAAGCC

−124 C > T /G > A mutation

G14

CCGGGGAAAGAACAGGACGCGCTCCCACGTGGCGGAGGGACTGGGGACCCGGGCACCCGTCCTGCCCCTTCACCTTCCA
GCTCCGCCTCCTCCGCGCGGACCCCGCCCCGTCCCGACCCCT**T**CCGGGTCCCCGGCCCAGCCCC**C**TCCGGGCCCTCC-
CAGCCCCTCCCCTTCCTTTCCGCGGCCCCGCCCTCTCCTCGCGGCGCGAGTTTCAGGCAGCGCTGCGTCCTGCTGCGCA

CGTGGGAAGCACATTTTATGATAATTTTGACGTTACTTATCATTTTTATACTGCATACATCCTAAGGACAAAAAACAAAAT-
TAAATCTGATTATCAACCTTTTCCGCGACAATATTTTTACAC

−146 C > T /G > A mutation

U3013

CTCCTTTACAGCCGGACGCGCTTCCACGTGGCGGAGGGACTGGGGACCCGGGCACCCGTCCTGCCCCTTCACCTTCCAGC
TCCGCCTCCTCCGCGCGGACCCCGCCCCGTCCCGACCCCT**C**CCGGGTCCCCGGCCCAGCCCC**T**TCCGGGCCCTCC-
CAGCCCCTCCCCTTCCTTTCCGCGGCCCCGCCCTCTCCTCGCGGCGCGAGTTTCAGGCAGCGCTGCGTCCTGCTGCG-
CACGTGGGAAGCCA

−124 C > T/G > A mutation

CRISPR-mediated insertion of hTERT promoter-driven gaussia luciferase in to the CCR5 locus

The hTERT promoter driven Gaussia Luciferase insert construct was obtained from a Genecopoeia promoter reporter clone. The insert sequence was cloned into AY10_pS. Donor.R5.TS. The hTERT promoter donor vector with mutation at – 124 position was generated using Quikchange SDM kit (Agilent) according to the manufacturers' protocol. For cleavage at CCR5 locus a reported gRNA sequence (5′-GGAGAGCTTGGCTCTGTTGGGGG-3′) was cloned into the pX459 v2.0, a gift from Feng Zhang that co-expresses cas9 protein and the gRNA. The gRNA cloned pX459 and the donor vector were co-transfected using FUGENE HD transfection agent according to the manufacturers' protocol. Starting from 36 hours post transfection, the cells were treated with 2ug/ml puromycin for 3 days for selecting cells that have taken up pX459 plasmid. After growing for 5 days after selection, the cells were seeded into 96 well plates after dilution for clonal selection. 40 clones were screened using gaussia luciferase activity and PCR to find out the positive clones.

Confirmation of CCR5-hTERT-Gaussia insert by sequencing and culture conditions

The inserted regions was PCR amplified with primers aligning to the CCR5 locus region flanking the *TERT*-Gaussia on both sides and sequenced.

In case of mutations, the inserted promoter was amplified (with primers flanking the CCR5 locus, as mentioned above) and confirmed by sequencing.

The highlighted bases in the following sequences correspond to −146 and −124 respectively from start of sequence (5′ to 3′ in the anti-sense strand). Green designates WT and purple designates mutated bases.

Post confirmation these cells were maintained in Dulbecco's Modified Eagle's Medium-High Glucose (DMEM-HG) supplemented with 10% FBS with addition of 1X anti-anti to cells post single cell seeding of CRISPR mutated pooled cell population.

CCR5 TERT –Gaussia insert WT

CGCCTCCTCCGCGCGGACCCCGCCCCGTCCCGACCCCTCCCGGGTCCCCG GCCCAGCCCCCTCCGGGCCCTCCCAGCCC
CTCCCCTTCCTTTCCGCGGCC

CCR5 TERT –Gaussia insert −124 C > T/G > A mutation

CGCCTCCTCCGCGCGGACCCCGCCCCGTCCCGACCCCTCCCGGGTCCCCG
GCCCAGCCCCTTCCGGGCCCTCCCAGCCCCTCCCCTTCCTTTCCGCGGCC

CCR5 TERT – Gaussia insert −146 C > T/G > A mutation

CGCCTCCTCCGCGCGGACCCCGCCCCGTCCCGACCCCTTCCGGGTCCCCG
GCCCAGCCCCCTCCGGGCCCTCCCAGCCCCTCCCCTTCCTTTCCGCGGCC

METHODS DETAILS

Analysis of TERT promoter sequence across vertebrates for G-quadruplex

G-quadruplex sequences were identified within ± 500 bp TERT TSS in various mammalian clades using reported Quadbase 2 server which detects G-quadruplexes from sequence (Dhapola and Chowdhury, 2016). Sequence homology and conservation scores were determined using neighbor joining cluster generation algorithm in the publicly available multiple sequence alignment tool MUSCLE (Edgar, 2004).

ChIP (chromatin immunoprecipitation)

ChIP assays were performed as per protocol previously reported in Mukherjee et al. (2018). ChIP assays were performed using relevant primary antibody. IgG was used for isotype control in all ChIP experiments. Three million cells were harvested and fixed for each were fixed with ~1% formaldehyde for 10 min and lysed. Chromatin was sheared to an average size of ~200-300 bp using Biorupter (Diagenode). 10% of sonicated fraction was processed as input using phenol–chloroform and ethanol precipitation. ChIP was performed using 3 μg of the respective antibody incubated overnight at 4°C. Immune complexes were collected using herring sperm

DNA-saturated Magnetic Dyna- beads (protein G/A) and washed extensively using a series of low salt, high salt and LiCl Buffers. The Dynabeads were then resuspended in TE (Tris- EDTA pH 8.1) buffer and incubated with proteinase K at 55°C for 1hr . Then, phenol-chloroform- isoamyl alcohol was utilized to extract DNA from the proteinase K treated fraction. DNA was precipitated by centrifugation after incubating overnight at −20°C with isopropanol with glycogen and 3M sodium acetate. The precipitated pellet was washes with freshly prepared 70% ethanol and resuspended in nuclease free water. ChIP DNA was further validated by q-PCR method.

Analysis of ChIP experiments-

For TRF2, REST and EZH2, ChIP-q-PCR was performed with equal amount of DNA (quantified by qubit HS DNA kit) from each ChIP and its respective mock (IgG). Thereafter respective mean Ct values were used for calculating fold change over IgG (mock).

For histone ChIP assays, ChIP-qPCR was performed with equal amount of DNA from each histone ChIP and its respective total H3 ChIP. This was normalized to 1% input. The input normalized mean Ct values for ChIP and total H3 were used for calculating fold change over total H3.

In case of BG4 ChIP, since the antibody was produced in *E. coli*, a no antibody mock control was used. Similar to the other ChIP assays, ChIP-qPCR was performed with equal amount of ChIP DNA and mock immunoprecipitation before calculating fold change over mock.

Tel PCR

Tel PCR was used as a positive control for TRF2 ChIP, as TRF2 is a bonafide Telomere binding protein. Following, Chromatin immunoprecipitation using Anti-TRF2 antibody, we performed a Real-Time PCR with equal amounts of DNA template form ChIP and IgG fractions, using telomere specific primers (O'Callaghan et al., 2008) at an annealing standardized at an annealing temperature of 52.5°C. The ChIP fraction readout was normalized over IgG to confirm if there was substantial TRF2 binding at the telomeres over background.

LSD1 chromatiniImmunoprecipitation

ChIP (Chromatin Immunoprecipitation) was performed using ChIP protocol same as above. LSD1 primary antibody (2139-CST anti-rabbit) was used – 3 μl per pull down along with respective Mock(IgG) immunoprecipitation.

Re-ChIP

For Re-ChIP of TRF2 immunoprecipitated fraction with REST, the above stated ChIP protocol was followed with a starting harvest of 6 million cells with pull-down of TRF2 mouse monoclonal antibody using protein-G-dynabeads. For Re-ChIP, half the pull-down fraction was resuspended in TE buffer with 10mM DTT after the salt buffer washes and incubated for 30 mins at RT. Following this the fraction was centrifuged at 10K rpm at 4°C for 10 mins and supernatant was used as lysate for REST ChIP using REST rabbit monoclonal antibody and pull down using protein A Dynabeads.

Immunoprecipitation of proteins

Six million cells were collected and washed in cold 1X PBS and lysed using RIPA (Sigma) with 1x mammalian Protease inhibitor Cocktail as per manufacturers' protocol. For immunoprecipitation experiments 1 mg of protein was incubated for 4 hours at 4°C with primary antibody in ratio recommended by manufacturer for immunoprecipitation. The pull-down was performed using Catch and Release co-immunoprecipitation kit (Millipore) as per manufacturer's protocol.

Immunofluorescence microscopy

Adherent cells were seeded on coverslips and allowed to reach a confluency of ~70%. Cells were fixed using freshly prepared 4% Paraformaldehyde by incubating for 10 min at RT. Cells were permeabilised with 0.5% Triton X-100 (10 min at RT) and treated with blocking solution (5% BSA in PBS) for 2 hr at RT. All the above stated were followed by three washes with ice cold PBS for 5 mins each. Post-blocking, cells treated with relevant antibodies as follows: anti-TRF2 antibody mouse (1:200), anti-hTERT antibody rabbit (1:200) and incubated overnight at 4°C in a humid chamber. Post-incubation, cells were washed alternately with PBS and PBST three times and probed with secondary Ab (rabbit Alexa Fluor® 488(1:1000) / mouse Alexa Fluor® 594 (1:1000)) for 2 hr at RT. Cells were washed again alternately with PBS and PBST three times and mounted with Prolong® Gold anti-fade reagent with DAPI. Images were taken on Leica TCS-SP8 confocal microscope. LEICA LAS-AF software was used to calculate TRF2 and hTERT signal intensity (a.u.) post (region of interest) ROI definitions for nuclear signal.

Immuno-flow cytometry

3 million cells for each condition were fixed using 4% formaldehyde for 10 mins at RT followed by 3 ice cold PBS washes for 5 mins each. Cells were permeabilised using 90% Methanol (pre-chilled) for 5 mins and followed by three ice cold PBS washes for 5 mins each. Dilution of primary antibodies were made (hTERT rabbit and TRF2 mouse) in 1% BSA (in PBS) in 1:250 ratio by volume. Cells were incubated with primary antibody cocktail for 2 hr at RT. Three ice cold PBS washes to cells (10 mins each) were given and secondary antibodies- rabbit Alexa Fluor® 488(1:1000) / mouse Alexa Fluor® 594(1:1000) in 1% BSA (in PBS) were added. Cells were incubated at RT for 1hr and given three ice cold PBS washes (10 mins each). Cells were resuspended in 0.5 mL of PBS and scored for

Fluorescence intensity in an Acuuri c6 flow cytometer in the FL1 (488 nm) and FL3 (594 nm) channels. The FCS files were analyzed using Flow-Jo (version 10) software.

Transfections and TRF2 silencing

Cells were transfected in a 1:3 complex of FUGENE HD and DNA/RNA using protocols previously described for TRF2 WT and mutant mammalian expression plasmids and TRF2 siRNA pool was used for TRF2 silencing at 150pMol concentration keeping cells treated with same concentration of scrambled RNA as control; as described in Mukherjee et al. (2018, 2019a) . Cells were incubated with transfection complex for 12 hours in media post which a media change was given. Cells were given fresh media changes every 24 hours. All experiments were performed following transient TRF2 silencing for 48hrs.

GABPA silencing

We transfected cells with siRNA against GABPA as published previously by Stern et al. (2015). A pool of four siRNAs used was at a concentration of 100pM, transfected using fugene. Following transfection we confirmed silencing using RT-PCR with primers to assess GABPA expression levels.

TRF2 silencing recovery experiment

Post Transfection with the TRF2 silencing siRNA-FUGENE complex, the transfection complex was removed from the HT1080 cells post 6hrs and fresh media change was given. One well was kept un-transfected; this was collected as 0hr time point. Transfected cells were collected post 18hrs after first media change; this was 24hr time point. A media change was given to the remaining cells at this stage and 24hr later the 48hr time point cells were collected. A final media change was given to the cells in the remaining well which were collect post next 24 hr as the 72hr time point. All the collected cells were stored in Tirzol and RNA isolation, cDNA synthesis and RT PCR for *TRF2* and *hTERT* gene expressions were performed together.

Gaussia-luciferase assay

Minimal promoter region of TERT (~1300 bp starting from 48 bp downstream of Transcription start site) procured from Genecopoeia-HPRM25711-PG04 (pEZX-PG04.1 vector) .Gaussia luciferase kit from Promega was used for detecting secreted Gaussia luciferase signal as per manufacturer's protocol.

Real time PCR for mRNA expression

Total RNA was isolated using TRIzol® Reagent (Invitrogen, Life Technologies) according to manufacturer's instructions. RNA was quantified and used for cDNA preparation using Applied Biosciences kit. A relative transcript expression level for genes was measured by quantitative real-time PCR using a SYBR Green based method. Average fold change was calculated by difference in threshold cycles (Ct) between test and control samples. *GAPDH* gene was used as housekeeping control for normalizing the cDNA concentration of each sample. Each experiment was performed in biological triplicates; where each time control and test conditions were set up separately and each sample was run in q-PCR thrice as technical replicates. Following this the technical replicates were averaged. We calculated the fold change of test over respective control conditions and designated the test condition as "1" for plotting; p values in all cases were calculated taking into conversation the variability of both the control and test readings.

Dot blot analysis

For dot blot analysis, Genomic/ ChIP DNA was denatured at 95°C and dot blotted on N+ hybond membrane (Amersham) in pre -wetted in 2X SSC buffer. The DNA was UV cross-linked. Membranes were pre-hybridized in Rapid-Hyb buffer (Amersham) for 30 min at 37°C. Following this, hybridization with a 24-bp radio-labeled telomeric probe (AATCCC)4 was performed for 4 hr at 37°C and membranes washed with 2X SSC and 0.2X SSC + 0.1% SDS twice at hybridization temperature before exposing overnight on phosphoimager imaging plate. All data were scanned using Bio-Rad Personal Molecular Imager. Data was processed and quantified using ImageJ image analysis software.

Western blotting

For western blot analysis, protein lysates were prepared by resuspending cell pellets in passive lysis buffer/RIPA with 1x mammalian Protease inhibitor Cocktail. Protein was separated using 10% SDS-PAGE and transferred to polyvinylidene difluoride membranes (Immobilon FL, Millipore). After blocking the membrane was incubated with primary antibodies- anti-TRF2 antibody (Novus Biological), anti-TERT antibody (Abcam), anti-REST(Millipore), anti-EZH2(CST) and anti-GAPDH antibody (Santa-cruz). Secondary antibodies, anti-mouse and anti-rabbit HRP conjugates were from CST. The blot was finally developed by using Millipore HRP chemiluminescence detection kit and images in a GE chemiluminescence imager.

G-quadruplex preparation

5 μM of oligonucleotide in each case was diluted in 10 mM Tris HCl ph7.5 and 140 mM KCl and denatured by heating to 95°C for 5 min and slowly cooled to 25°C for overnight.

Circular dichroism

The circular dichroism (CD) spectra were recorded on a Jasco-810 Spectropolarimeter equipped with a Peltier temperature controller. Experiments were carried out using a 1 mm path-length cuvette over a wavelength range of 200-330 nm. The G-quadruplex formation was induced as described above, and the G-quadruplexes formed were used as such for monitoring the CD spectra. The CD spectra reported are representations of three averaged scans taken at 25°C and are baseline corrected for signal contributions due to the buffer.

In the CD experiments performed with the ligand and TRF2 purified protein. First, the CD spectra of the 5uM solution (in quadruplex buffer) of mutant hTERT promoter oligo (G-quadruplex) was recorded. This was followed by taking a blank reading for buffer+ protein/ligand. Meanwhile, the hTERT promoter mutant oligos were incubated with 5 times higher molar concentration of ligand or protein. The ligand/protein and the oligos were mixed well and then allowed to be incubated for 20min after which their CD spectra were recorded again.

ELISA

5′-biotinylated oligonucleotides were induced to form G-quadruplex as described above. The 5 uM G-quadruplex stock solution was diluted to a final concentration of 50 pM in 1X Tris-buffer saline, 0.1% Tween 20 (TBST) buffer; 20 ul of this was loaded into each well of a 384 well streptavidin coated pre-blocked plate from Thermo Scientific (Pierce) and incubated at 37°C on shaker for 2 hours to allow streptavidin and biotin binding. Following this the excess unbound oligonucleotides was washed off using 1XTBST buffer X3 washes.

TRF2 protein was diluted in 1X Phosphate buffer saline, 0.1% Tween 20 (PBST) buffer and 20ul of dissolved protein was incubated with bound quadruplex (in the wells) in increasing concentration across wells for 2 hours on shaker at 4°C. Unbound protein was washed off with 1X PBST buffer X3 washes. Anti-TRF2 antibody (Novus) was used at 1:1000 dilution (20 μl per well) and incubated for 1 hr at room temperature on shaker. Wells were washed three times with 1X PBST. Alkaline phosphatase conjugated Anti-IgG antibody (Sigma) was used at 1:1000 dilution (20 μl/well) and incubated for 45 minutes at room temperature on shaker and then wells were washed once with 1X PBST and twice with 1X PBS. 20 μl BCIP/NBT substrate was added into each well and absorbance was recorded at 610 nm wavelength for 1hour with 10 min interval on TECAN multimode reader. GraphPad Prism7 was used for analysis.

Telomerase activity using ELISA TRAP

One million cells were lysed using CHAPS lysis buffer provided in the kit, we add RNase inhibitor and protease inhibitor to avoid and protein degradation. Post lysate preparation protein concentration is estimated. Following this all protein samples were diluted to 0.5ug/ul concentration so a uniform volume of 2ul could be picked to add 1ug of lysate for TRAP assay as guided in the protocol. As a precaution we performed a second round of protein estimation here to confirm our dilutions were to an exact 0.5ug/ul concentration. Next telomerase repeat amplification protocol (TRAP) (Kim et al., 1994) PCR was performed using PCR master mix provided in the kit. The primers were AG$(GGTTAG)_7$ sequence repeats 3′biotnylated P1-TS primers. This allows telomerase to add the substrate TTAGGG six-mer substrate on the P1-TS primers, substrate primers a $(TTAGGG)_6$ repetitive sequences- P2. P3 is dioxygenin tagged used to amplify the telomeric sequence to a specific number of cycles. Post PCR as per the protocol conditions, the product is estimated using ELISA performed on streptavidin coated plate using anti-dig-Pod antibody using ROCHE TeloTAGGG Telomerase PCR ELISA kit. The method is well reported (Giri et al., 2010; Shi et al., 2014).

Oligonucleotide-pulldown assay

Total cell lysate of > 2000ug concentration was isolated using RIPA buffer (without SDS) with 1X mPIC. Lysate was pre-cleared for cellular biotin by adding 60ul of Dynabeads MyOne Streptavidin C1 (cat no65001) beads per sample and rotating at 4-degree celsius for 2 hours. Streptavidin beads were then removed using a magnetic stand and the lysate was divided into two equal parts. To one the wild-type biotinylated oligonucleotide was added, while to the other mutant biotinylated oligonucleotide was added, amounting to 50 pmoles in each. The lysate was incubated on rotor with oligonucleotides for 16hrs at 4°C. Thereafter the protein and DNA were cross-linked for 15min in UV crosslinker. Thereafter 100ul of Streptavidin beads were added to each tube post twice washing of beads in 1XPBST. Beads were incubated with cross-liked lysate for 2 hours. Post this, beads were separated on magnetic stand and washed twice in 1X wash buffer (20 mM Tris+10mM NaCl+ Tween 0.1%). Lastly the bound protein was eluted using Elution buffer (1MTris HCl pH6.8+10% SDS+ Bitoin 25mM). The beads were re-suspended in 50ul of elution buffer and heated at 95°C for 5 min, the buffer was then stored in fresh tube, the process was repeated with 50ul of elution buffer. Of this total eluted protein, 60ul was run on SDS-PAGE gel after adding 6X protein loading dye, as in a normal western blot protocol.

TRF2 ChIP-seq coverage on TERT promoter

Sorted Alignment files (BAM) for TRF2 ChIP-seq (Mukherjee et al., 2019a) was visualized using the publicly available software IGV for Coverage of reads on h*TERT* promoter with Transcription start site (TSS) defined using transcript variant NM_198253 (RefSeq).

QUANTIFICATION AND STATISTICAL ANALYSIS

All experiments were performed in three biological replicates. Based on the triplicate readings all error bars represent ± standard deviations from mean values; p values calculated. For a comparison of two datasets (control and TRF2 silenced conditions) we compared using paired/unpaired t test. Further multiple comparisons were performed using two-way ANOVA (*$p < 0.05$, **$p < 0.01$, ***$p < 0.005$, ****$p < 0.0001$). All the calculations were performed using Prism Graphpad, which was also used to plot all datasets.